Anaerobic sulfur oxidation underlies adaptation of a chemosynthetic symbiont to oxic-anoxic interfaces

Running title: chemosynthetic ectosymbiont's response to oxygen

Gabriela F. Paredes[1], Tobias Viehboeck[1,2], Raymond Lee[3], Marton Palatinszky[2], Michaela A. Mausz[4], Sigfried Reipert[5], Arno Schintlmeister[2,6], Jean-Marie Volland[1,‡], Claudia Hirschfeld[7] Michael Wagner[2,8], David Berry[2,9], Stephanie Markert[7], Silvia Bulgheresi[1,*] and Lena König[1,*]

[1] University of Vienna, Department of Functional and Evolutionary Ecology, Environmental Cell Biology Group, Vienna, Austria

[2] University of Vienna, Center for Microbiology and Environmental Systems Science, Division of Microbial Ecology, Vienna, Austria

[3] Washington State University, School of Biological Sciences, Pullman, WA, USA

[4] University of Warwick, School of Life Sciences, Coventry, UK

[5] University of Vienna, Core Facility Cell Imaging and Ultrastructure Research, Vienna, Austria

[6] University of Vienna, Center for Microbiology and Environmental Systems Science, Large-Instrument Facility for Environmental and Isotope Mass Spectrometry, Vienna, Austria

[7] University of Greifswald, Institute of Pharmacy, Department of Pharmaceutical Biotechnology, Greifswald, Germany

[8] Aalborg University, Department of Chemistry and Bioscience, Aalborg, Denmark

[9] Joint Microbiome Facility of the Medical University of Vienna and the University of Vienna, Vienna, Austria

[‡] Present affiliation: Joint Genome Institute/Global Viral, San Francisco, CA, USA

Corresponding Authors

Silvia Bulgheresi: University of Vienna, Department of Functional and Evolutionary Ecology, Environmental Cell Biology Group, Althanstrasse 14, 1090 Vienna, Austria, +43-1-4277-76514, silvia.bulgheresi@univie.ac.at

Lena König: University of Vienna, Department of Functional and Evolutionary Ecology, Environmental Cell Biology Group, Althanstrasse 14, 1090 Vienna, Austria, +43-1-4277-76527, lena.koenig@univie.ac.at

* These authors contributed equally to this work.

Competing Interests

The authors declare no competing financial interest.

Abstract

Chemosynthetic symbioses occur worldwide in marine habitats. However, physiological studies of chemoautotrophic bacteria thriving on animals are scarce. *Stilbonematinae* are coated by monocultures of thiotrophic Gammaproteobacteria. As these nematodes migrate through the redox zone, their ectosymbionts experience varying oxygen concentrations. Here, by applying omics, Raman microspectroscopy and stable isotope labeling, we investigated the effect of oxygen on the metabolism of *Candidatus* Thiosymbion oneisti. Unexpectedly, sulfur oxidation genes were upregulated in anoxic relative to oxic conditions, but carbon fixation genes and incorporation of ^{13}C-labeled bicarbonate were not. Instead, several genes involved in carbon fixation, the assimilation of organic carbon and polyhydroxyalkanoate (PHA) biosynthesis, as well as nitrogen fixation and urea utilization were upregulated in oxic conditions. Furthermore, in the presence of oxygen, stress-related genes were upregulated together with vitamin and cofactor biosynthesis genes likely necessary to withstand its deleterious effects.

Based on this first global physiological study of a chemosynthetic ectosymbiont, we propose that, in anoxic sediment, it proliferates by utilizing nitrate to oxidize reduced sulfur, whereas in superficial sediment it exploits aerobic respiration to facilitate assimilation of carbon and nitrogen to survive oxidative stress. Both anaerobic sulfur oxidation and its decoupling from carbon fixation represent unprecedented adaptations among chemosynthetic symbionts.

Introduction

At least six animal phyla and numerous lineages of bacterial symbionts belonging to Alpha-, Delta-, Gamma- and Epsilonproteobacteria engage in chemosynthetic symbioses, rendering the evolutionary success of these associations incontestable [1, 2]. Many of these mutualistic associations rely on sulfur-oxidizing (thiotrophic), chemoautotrophic bacterial symbionts, that oxidize reduced sulfur compounds for energy generation in order to fix inorganic carbon (CO_2) for biomass build-up. Particularly in binary symbioses involving

intracorporeal thiotrophic bacteria, it is generally accepted that the endosymbiont's chemosynthetic metabolism serves to provide organic carbon for feeding the animal host [reviewed in 1–3]. In addition, some chemosynthetic symbionts have been found capable to fix atmospheric nitrogen, albeit symbiont-to-host transfer of fixed nitrogen remains unproven [4, 5]. As for the rarer chemosynthetic bacterial-animal associations in which symbionts colonize exterior surfaces (ectosymbionts), fixation of inorganic carbon and transfer of organic carbon to the host has only been demonstrated for the microbial community colonizing the gill chamber of the hydrothermal vent shrimp *Rimicaris exoculata* [6].

In this study, we focused on *Candidatus* Thiosymbion oneisti, a Gammaproteobacterium belonging to the basal family of *Chromatiaceae* (also known as purple sulfur bacteria), which colonizes the surface of the marine nematode *Laxus oneistus* (*Stilbonematinae*). Curiously, this group of free-living roundworms represents the only known animals engaging in monospecific ectosymbioses, i.e. each nematode species is ensheathed by a single *Ca.* Thiosymbion phylotype, and, in the case of *Ca*. T. oneisti, the bacteria form a single layer on the cuticle of its host [7–11]. Moreover, the rod-shaped representatives of this bacterial genus, including *Ca*. T. oneisti, divide by FtsZ-based longitudinal fission, a unique reproductive strategy which ensures continuous and transgenerational host-attachment [12–14].

Like other chemosynthetic symbionts, *Ca*. Thiosymbion have been considered chemoautotrophic sulfur oxidizers based on several lines of evidence: stable carbon isotope ratios of symbiotic nematodes are comparable to those found in other chemosynthetic symbioses [15]; the key enzyme for carbon fixation via the Calvin-Benson-Bassham cycle (RuBisCO) along with enzymes involved in sulfur oxidation and elemental sulfur have been detected [16–18]; reduced sulfur compounds (sulfide, thiosulfate) have been shown to be taken up from the environment by the ectosymbionts, to be used as energy source, and to be responsible for the white appearance of the symbiotic nematodes [18–20]; the animals often occur in the sulfidic zone of marine shallow-water sands [21]. More recently, the

phylogenetic placement and genetic repertoire of *Ca*. Thiosymbion species have equally been supporting the chemosynthetic nature of the symbiosis [5, 11].

The majority of thioautotrophic symbioses have been described to rely on reduced sulfur compounds as electron donors and oxygen as terminal electron acceptor [2, 3]. However, given that sulfidic and oxic zones are often spatially separated, also owing to abiotic sulfide oxidation [22, 23], chemosynthetic symbioses (1) are found where sulfide and oxygen occur in close proximity (e.g., hydrothermal vents, shallow-water sediments) and (2) host behavioral, physiological and anatomical adaptations are needed to enable thiotrophic symbionts to access both substrates. Host-mediated migration across the substrate gradients is perhaps the most commonly encountered behavioral adaptation and was proposed for deep-sea crustaceans, as well as for shallow water interstitial invertebrates and *Kentrophoros* ciliates [reviewed in 1, 2]. Also the symbionts of *Stilbonematinae* have long been hypothesized to associate with their motile nematode hosts to maximize sulfur oxidation-fueled chemosynthesis, by alternately accessing oxygen in superficial sand and sulfide in deeper, anoxic sand. This hypothesis was based upon the distribution pattern of *Stilbonematinae* in sediment cores together with movement patterns in experimental columns [15, 19, 21]. However, *Ca.* T. oneisti and other chemosynthetic symbionts were subsequently shown to use nitrate as an alternative electron acceptor, and nitrate respiration was stimulated by sulfide, suggesting that some of the symbionts are capable of gaining energy by respiring nitrate instead of oxygen [20, 24–26].

Physiological studies are scarce because chemosynthetic associations remain difficult to cultivate. Importantly, the impact of anoxic and oxic conditions on central metabolic processes of the symbionts has not yet been investigated. This knowledge gap is particularly remarkable in view of the exposed location of ectosymbionts, which leaves them less sheltered than endosymbionts in the face of fluctuating concentrations of substrates for energy generation. To understand how oxygen affects thiotrophy, we incubated symbiotic nematodes associated with *Ca*. T. oneisti under different conditions resembling their natural environment, and subsequently examined the ectosymbiont's transcriptional responses via

RNA sequencing (RNA-Seq). In combination with complementary methods such as stable isotope-labeling, proteomics, Raman microspectroscopy and lipidomics, we show that the ectosymbiont exhibits specific metabolic responses to anoxic and oxic conditions. Most strikingly, sulfur oxidation but not carbon fixation was upregulated in anoxia. This overturns the current opinion that sulfur oxidation requires oxygen and drives carbon fixation in chemosynthetic symbioses. We finally present a metabolic model of a thiotrophic ectosymbiont experiencing an ever-changing environment and propose that anaerobic sulfur oxidation coupled to denitrification represents the ectosymbiont's preferred metabolism for growth.

Materials and Methods

Sample collection

Laxus oneistus individuals were collected on multiple field trips (2016-2019) at approximately 1 m depth from sand bars off the Smithsonian Field Station, Carrie Bow Cay in Belize (16°48′11.01″N, 88°4′54.42″W). The nematodes were extracted from the sediment by gently stirring the sand and pouring the supernatant seawater through a 212 µm mesh sieve. The retained meiofauna was collected in a petri dish, and single worms of similar size (1-2 mm length, representing adult *L. oneistus*) were handpicked by forceps (Dumont 3, Fine Science Tools, Canada), under a dissecting microscope. Right after collection, the nematodes were used for various incubations as described below.

Sediment cores analysis

The habitat and spatial distribution of *L. oneistus* were characterized by sediment core analyses. Sediment pore-water was collected in July 2017, in 6 cm intervals down to a depth of 30 cm, by using cores of 60 cm length and 60 mm diameter (UWITEC, Mondsee, Austria), connected to rhizon samplers of a diameter of 2.5 mm and mean pore size of 0.15 µm (Rhizosphere Research Products, Wageningen, Netherlands). In total, nine sediment cores

were randomly sampled on different days and at different spots in shallow, submerged sediment.

Immediately after collection, the sulfide content ($\sum H_2S$, i.e. the sum of H_2S, HS^- and S^{2-}) was determined by the methylene-blue method [27]. In short, 670 µl of a 2% zinc acetate solution was mixed with 335 µl sample and subsequently 335 µl 0.5% *N*,*N*-Dimethyl-*p*-phenylenediamine and 17 µl of 10% ferrous ammonium sulfate added and incubated for 30 min in the dark. Surface seawater was used as a blank. Absorbance was measured at 670 nm and concentrations were quantified via calibration (measurement of $\sum H_2S$ standard solutions in the concentration range from 0 to 0.5 mM $\sum H_2S$). Samples for dissolved inorganic nitrogen (DIN: nitrate, nitrite, and ammonia) measurements were stored and transported at -80°C, and analyzed at the University of Vienna, Austria. Nitrate (NO_3^-) and nitrite (NO_2^-) concentrations were determined according to the Griess method [28] using VCl_3 [29], whereas the concentration of ammonium (NH_4^+) was measured after Solórzano [30]. For the quantification of nitrate, nitrite and, ammonia, freshly prepared KNO_3, $NaNO_2$ and NH_4Cl solutions ranging from 0 to 20 µM were used to create standard curves, respectively. Artificial seawater served as a blank [prepared after 31] and all measurements were performed in triplicates. Rapidly after pore-water sampling, the abundance of *L. oneistus* was determined within 6 cm-wide subsections of the cores. Each fraction was stirred separately, and the supernatant decanted through a 212 µm-mesh sieve. The nematodes were counted under a dissecting microscope. Mean nematode abundances and $\sum H_2S$ concentrations are shown in Figure S1A. All measurements data are listed in Table S1.

Incubations for RNA sequencing (RNA-Seq)

To analyze the physiological response of *Ca*. T. oneisti to oxygenated and reducing conditions, three batches of 50 freshly collected *L. oneistus* individuals were incubated for 24 h in the dark, in either the presence (oxic) or absence (anoxic) of oxygen, in 13 ml-exetainers (Labco, Lampeter, Wales, UK) fully filled with 0.2 µm filtered seawater, respectively (Figure S1B). The oxic incubations consisted of two separate experiments of

196 low (hypoxic) and high (oxic saturated) oxygen concentrations. Here, all exetainers were
197 kept open, but only the samples with high oxygen concentrations were submerged in an
198 aquarium constantly bubbled with air (air pump plus; Sera, Heinsberg, Germany). Hypoxic
199 samples were exposed to air, and they started with around 130 µM O_2 but reached less than
200 60 µM O_2 after 24 h of incubation. This likely occurred due to nematode oxygen
201 consumption. On the other hand, the anoxic treatments comprised incubations to which
202 either 11 µM of sodium sulfide (Na_2S*9H_2O; Sigma-Aldrich, St. Louis, MS, USA) was added,
203 or no sulfide was supplied (Figure S1B), and $\sum H_2S$ concentrations were checked at the
204 beginning and at the end (24 h) of each incubation by spectrophotometric determination
205 following the protocol of Cline (see above). Anoxic incubations were achieved with the aid of
206 a polyethylene glove bag (AtmosBag; Sigma-Aldrich) that was flushed with N_2 gas (Fabrigas,
207 Belize City, Belize), together with incubation media and all vials, for at least 1 h before
208 closing. Dissolved oxygen inside the bag, and of every incubation was monitored throughout
209 the 24 h incubation time using a PreSens Fibox 3 trace fiber optic oxygen meter and non-
210 invasive trace oxygen sensor spots attached to the exetainers (PSt6 and PSt3; PreSens,
211 Regensburg, Germany). For exact measurements of $\sum H_2S$ and oxygen see Table S2.
212 Temperature and salinity remained constant throughout all incubations measuring 27-28°C
213 and 33-34 ‰, respectively. After the 24 h incubations, each set of 50 worms was quickly
214 transferred into 2 ml RNA storage solution (13.3 mM EDTA disodium dihydrate pH 8.0, 16.6
215 mM sodium citrate dihydrate, 3.5 M ammonium sulfate, pH 5.2), kept at 4°C overnight, and
216 finally stored in liquid nitrogen until RNA extraction.
217

218 **RNA extraction, library preparation and RNA-Seq**

219 RNA was extracted using the NucleoSpin RNA XS Kit (Macherey-Nagel**,** Düren, Germany).
220 Briefly, sets of 50 worms in RNA storage solution were thawed and the worms were
221 transferred into 90 µl lysis buffer RA1 containing Tris (2-carboxyethyl) phosphine (TCEP)
222 according to the manufacturer. The remaining RNA storage solution was centrifuged to
223 collect any detached bacterial cells (10 min, 4°C, 16 100 x g), pellets were resuspended in

224 10 µl lysis buffer RA1 (plus TCEP) and then added to the worms in lysis buffer. To further
225 disrupt cells, suspensions were vortexed for two minutes followed by three cycles of freeze
226 (-80°C) and thaw (37°C), and homogenization using a pellet pestle (Sigma-Aldrich) for 60 s
227 with a 15 s break after 30 s. Any remaining biological material on the pestle tips was
228 collected by rinsing the tip with 100 µl lysis buffer RA1 (plus TCEP). Lysates were applied to
229 NucleoSpin Filters and samples were processed as suggested by the manufacturer,
230 including an on-filter DNA digest. RNA was eluted in 20 µl RNase-free water. To remove any
231 residual DNA, a second DNase treatment was performed using the Turbo DNA-free Kit
232 (Thermo Fisher Scientific, Waltham, MA, USA), RNA was then dissolved in 17 µl RNase-free
233 water, and the RNA quality was assessed using a Bioanalyzer (Agilent, Santa Clara, CA,
234 USA). To check whether all DNA was digested, real-time quantitative PCR using the GoTaq
235 qPCR Master Mix (Promega, Madison, WI, USA) was performed targeting a 158 bp stretch
236 of the *sodB* gene using primers specific for the symbiont (sodB-F:
237 GTGAAGGGTAAGGACGGTTC, sodB-R: AATCCCAGTTGACGATCTCC, 10 µM per
238 primer). Different concentrations of genomic *Ca.* T. oneisti DNA were used as positive
239 controls. The program was as follows: 1x 95°C for 2 min, 40x 95°C for 15 s and 60°C for 1
240 min, 1x 95°C for 15 s, 55°C to 95°C over 20 min. Next, bacterial and eukaryotic rRNA was
241 removed using the Ribo-Zero Gold rRNA Removal Kit (Epidemiology) (Illumina, San Diego,
242 CA, USA) following the manufacturer's instructions, but volumes were adjusted for low input
243 RNA [32]. In short, 125 µl of Magnetic Beads Solution, 32.5 µl Magnetic Bead Resuspension
244 Solution, 2 µl Ribo-Zero Reaction Buffer and 4 µl Ribo-Zero Removal Solution were used
245 per sample. RNA was cleaned up via ethanol precipitation, dissolved in 9 µl RNase-free
246 water, and rRNA removal was evaluated using the Bioanalyzer RNA Pico Kit (Agilent, Santa
247 Clara, CA, USA). Strand-specific, indexed cDNA libraries were prepared using the SMARTer
248 Stranded RNA-Seq Kit (Takara Bio USA, Mountain View, CA, USA). Library preparation was
249 performed according to the instructions, with 8 µl of RNA per sample as input, 3 min
250 fragmentation time, two rounds of AMPure XP Beads (Beckman Coulter, Brea, CA, USA)
251 clean-up before amplification, and 18 PCR cycles for library amplification. The quality of the

252 libraries was assessed via the Bioanalyzer DNA High Sensitivity Kit (Agilent). Libraries were
253 sequenced on an Illumina HiSeq 2500 instrument (single-read, 100 nt) at the next
254 generation sequencing facility of the Vienna BioCenter Core Facilities (VBCF,
255 https://www.viennabiocenter.org/facilities/).
256
257 **Genome sequencing, assembly and functional annotation**
258 The genome draft of *Ca.* T. oneisti was obtained by performing a hybrid assembly using
259 reads from Oxford Nanopore Technologies (ONT) sequencing and Illumina sequencing. To
260 extract DNA for ONT sequencing and dissociate the ectosymbionts from the host,
261 approximately 800 *Laxus oneistus* individuals were incubated three times for 5 min each in
262 TE Buffer (10 mM Tris-HCl pH 8.0, 1 mM disodium EDTA pH 8). Dissociated symbionts
263 were collected by 10 min centrifugation at 7 000 x g and subsequent removal of the
264 supernatant. DNA was extracted from this pellet using the Blood and Tissue Kit (Qiagen,
265 Hilden, Germany) according to the manufacturer's instructions. The eluant was further
266 purified using the DNA Clean & Concentrator-5 kit (Zymo Research, Irvine, CA, USA), and
267 the DNA was eluted twice with 10 µl nuclease free water.
268 The library for ONT sequencing was prepared using the ONT Rapid Sequencing kit
269 (SQK RAD002) and sequenced on a R9.4 flow cell (FLO-MIN106) on a MinION for 48 h.
270 Base calling was performed locally with ONT's Metrichor Agent version 1.4.2, and resulting
271 fastq-files were trimmed using Porechop version 0.2.1 (https://github.com/rrwick/Porechop).
272 Illumina sequencing reads originate from a previous study [5], and were made available by
273 Harald Gruber-Vodicka at the MPI Bremen. Raw reads were filtered: adapters removed and
274 trimmed using bbduk (BBMap version 37.22, https://sourceforge.net/projects/bbmap/), with a
275 minimum length of 36 and a minimum phred score of 2. To only keep reads derived from the
276 symbiont, trimmed reads were mapped onto the available genome draft (NCBI Accession
277 FLUZ00000000.1) using BWA-mem version 0.7.16a-r1181 [33]. Reads that did not map
278 were discarded. The hybrid assembly was performed using SPAdes version 3.11 [34] with
279 flags --careful and the ONT reads supplied as --nanopore. Contigs smaller than 200 bp and

280 a coverage lower than 5X were filtered out with a custom python script. The genome
281 completeness was assessed using checkM version 1.0.18 [35] with the
282 gammaproteobacterial marker gene set using the taxonomy workflow. The genome was
283 estimated to be 96.63% complete, contain 1.12% contamination, and was 4.35 Mb in length
284 on 401 contigs with a GC content of 58.7%.

285 The genome of *Ca.* T. oneisti was annotated using the MicroScope platform [36],
286 which predicted 5 169 protein-coding genes. To expand the functional annotation provided
287 by MicroScope, predicted proteins were assigned to KEGG pathway maps using
288 BlastKOALA and KEGG Mapper-Reconstruct Pathway [37], gene ontology (GO) terms using
289 Blast2GO version 5 [38] and searched for Pfam domains using the hmmscan algorithm of
290 HMMER 3.0 [39, 40]. All proteins and pathways mentioned in the manuscript were manually
291 curated. Functional annotations can be found in Data S1.

292

293 **Gene expression analyses**

294 Based on quality assessment of raw sequencing reads using FastQC [41] and prinseq [42],
295 reads were trimmed and filtered using Trimmomatic [43] as follows: 15-24 nucleotides were
296 removed from the 5-prime end (HEADCROP), Illumina adapters were cut
297 (ILLUMINACLIP:TruSeq3-SE.fa:2:30:10), and only reads longer than 24 nucleotides were
298 kept (MINLEN). Mapping and expression analysis were done as previously described [44].
299 Briefly, reads were mapped to the *Ca.* T. oneisti genome draft using BWA-backtrack [33]
300 with default settings, only uniquely mapped reads were kept using SAMtools [45], and the
301 number of strand-specific reads per gene were counted using HTSeq in the union mode of
302 counting overlaps [46]. On average, 1.3 x 10^6 (3.5%) reads uniquely mapped to the *Ca.* T.
303 oneisti genome. For detailed read and mapping statistics see Figure S2A. Gene expression
304 and differential expression analysis was conducted using the R software environment and
305 the Bioconductor package edgeR [47–49]. Genes were considered expressed if at least two
306 reads in at least two replicates of one of the four conditions could be assigned. Replicate 3
307 of the hypoxic incubations was excluded from further analyses because gene expression

308 was very different compared to the other two replicates (Figure S2B). Including all four
309 conditions, we found 88.8% of total predicted symbiont protein-encoding genes to be
310 expressed (4 591 genes out of 5 169). Log_2TPM (transcripts per kilobase million) values per
311 gene and replicate were calculated and averages were determined per condition to estimate
312 expression strength. Median gene expression was determined from average log_2TPMs to
313 highlight expression trends of entire metabolic processes and pathways. Expression of
314 genes was considered significantly different if their expression changed two-fold between
315 two conditions with a false-discovery rate (FDR) ≤ 0.05 [50]. Throughout the paper, all genes
316 meeting these thresholds are either termed up- or downregulated or differentially expressed.
317 However, most follow-up analyses were conducted only considering differentially expressed
318 genes between the anoxic, sulfidic (AS) condition and both oxygenated conditions combined
319 (O, see Results and Figure S2C). Heatmaps show mean centered expression values to
320 highlight gene expression change.
321

322 **Bulk $\delta^{13}C$ isotopic analysis by Isoprime isotope ratio mass spectrometry (EA-IRMS)**

323 To further analyze the carbon metabolism of *Ca.* T. oneisti, specifically the assimilation of
324 carbon dioxide (CO_2) by the symbionts in the presence or absence of oxygen, batches of 50
325 freshly collected, live worms were incubated for 24 h in 150 ml of 0.2 µm-filtered seawater,
326 supplemented with 2 mM (final concentration) of either ^{12}C- (natural isotope abundance
327 control) or ^{13}C-labelled sodium bicarbonate (Sigma-Aldrich, St. Louis, MS, USA). In addition,
328 a second control was set up (dead control), in which prior to the 24 h incubation with ^{13}C-
329 labelled sodium bicarbonate, 50 freshly collected worms were chemically killed by fixing
330 them for 12 h in a 2% PFA/water solution.

331 All three incubations were performed in biological triplicates or quadruplets and set
332 up under anoxic, sulfidic and oxic conditions. Like the RNA-Seq experiment, the oxic
333 incubations consisted of two separate experiments of low (hypoxic) and high (oxic saturated)
334 oxygen concentrations. To prevent isotope dilution through exchange with the atmosphere,
335 both the oxic and anoxic incubations remained closed throughout the 24 h. The procedure

336 was as follows: 0.2 µm-filtered anoxic seawater was prepared as described above and was
337 subsequently used for both oxic and anoxic incubations. Then, compressed air (DAN oxygen
338 kit, Divers Alert Network, USA) and 25 µM of sodium sulfide (Na_2S*9H_2O; Sigma-Aldrich, St.
339 Louis, MS, USA) were injected into the oxic and anoxic incubations, respectively, to obtain
340 concentrations resembling the conditions applied in incubations for the RNA-Seq experiment
341 (see Table S2 for details about the incubation conditions and a compilation of the
342 measurement data).

343 At the end of each incubation (24 h), the nematodes were weighed (0.3-0.7 mg dry
344 weight) into tin capsules (Elemental Microanalysis, Devon, United Kingdom) and dried at
345 70°C for at least 24 h. Samples were analyzed using a Costech (Valencia, CA USA)
346 elemental analyzer interfaced with a continuous flow Micromass (Manchester, UK) Isoprime
347 isotope ratio mass spectrometer (EA-IRMS) for determination of $^{13}C/^{12}C$ isotope ratios.
348 Measurement values are displayed in δ notation [per mil (‰)]. A protein hydrolysate,
349 calibrated against NIST reference materials, was used as a standard in sample runs. The
350 achieved precision for $\delta^{13}C$ was ± 0.2 ‰ (one standard deviation of 10 replicate
351 measurements on the standard).

352

353 **Raman microspectroscopy**

354 Three individual nematodes per EA-IRMS incubation were fixed and stored in 0.1 M Trump's
355 fixative solution (0.1 M sodium cacodylate buffer, 2.5% GA, 2% PFA, pH 7.2, 1 000 mOsm L^{-}
356 ^{1}) [51], and washed three times for 10 min in 1x PBS (137 mM NaCl, 2.7 mM KCl, 10 mM
357 Na_2HPO_4, 1.8 mM KH_2PO_4, pH 7.4) before their ectosymbionts were dissociated by
358 sonication for 40 s in 10 µl 1x PBS. 1 µl of each bacterial suspension was spotted on an
359 aluminum-coated glass slide and measured with a LabRAM HR Evolution Raman
360 microspectroscope (Horiba, Kyoto, Japan). 50 individual single-cell spectra were measured
361 from each sample. All spectra were aligned by the phenylalanine peak, baselined using the
362 Sensitive Nonlinear Iterative Peak (SNIP) algorithm of the R package "Peaks"
363 (https://www.rdocumentation.org/packages/Peaks/versions/0.2), and normalized by total

364 spectrum intensity. For calculating the relative sulfur content, the average intensity value for
365 212-229 wavenumbers (S_8 peak) was divided by the average intensity of the adjacent flat
366 region of 231-248 wavenumbers [18]. For calculating the relative polyhydroxyalkanoate
367 (PHA) content, the average intensity value for 1 723-1 758 wavenumbers (PHA peak) was
368 divided by the average intensity of the adjacent flat region of 1 759-1 793 wavenumbers [52].
369 Median relative sulfur and PHA content (shown as relative Raman intensities) were
370 calculated treating all individual symbiont cells per condition as replicates. Statistically
371 significant differences were determined applying the Wilcoxon rank sum test.
372
373 **Assessment of the percentage of dividing cells**
374 Samples were fixed and ectosymbionts were dissociated from their hosts as described
375 above for Raman microspectroscopy. 1.5 µl of each bacterial suspension per condition were
376 applied to a 1% agarose covered slide [53] and cells were imaged using a Nikon Eclipse NI-
377 U microscope equipped with an MFCool camera (Jenoptik). Images were obtained using the
378 ProgRes Capture Pro 2.8.8 software (Jenoptik) and processed with ImageJ [54]. Bacterial
379 cells were manually counted (> 600 per sample), and grouped into constricted (dividing) and
380 non-constricted (non-dividing) cells based on visual inspection [14]. The percentage of
381 dividing cells was calculated by counting the total number of dividing cells and the total
382 amount of cells per condition. Statistical tests were performed using the Fisher's exact test.
383
384 **Data availability.** The assembled and annotated genome of *Ca*. T. oneisti has been
385 deposited at DDBJ/ENA/GenBank under the accession JAAEFD000000000. RNA-Seq data
386 are available at the Gene Expression Omnibus (GEO) database and are accessible through
387 accession number GSE146081
388
389 **Results**
390
391 **Hypoxic and oxic conditions induce similar expression profiles**

To understand how the movement of the animal host across the chemocline affects symbiont physiology and metabolism, we exposed symbiotic worms to sulfide (thereafter used for $\sum H_2S$) and oxygen concentrations resembling the ones encountered by *Ca.* T. oneisti in its natural habitat. Previous studies showed that *Stilbonematinae* live predominantly in anoxic sediment zones with sulfide concentrations < 50 µM [21]. To assess whether this applies to *Laxus oneistus* (i.e. *Ca.* T. oneisti's host) at our collection site (Carrie Bow Cay, Belize), we determined the nematode abundance relative to the sampling depth and sulfide concentration. We found all *L. oneistus* individuals in pore water containing ≤ 25 µM sulfide and only 2% of them living in non-sulfidic (0 µM sulfide) surface layers (Figure S1A, Table S1). Therefore, we chose anoxic seawater supplemented with ≤ 25 µM sulfide as the optimal incubation medium (AS condition). To assess the effect of oxygen on symbiont physiology, we additionally incubated the nematodes in hypoxic (< 60 µM oxygen) and oxygen-saturated (>100 µM) seawater. Nitrate, nitrite and ammonium could be detected throughout the sediment core including the surface layer (Table S1).

Differential gene expression analysis comparing hypoxic and oxygen-saturated incubations revealed that expression levels of 97.1% of all expressed genes did not significantly differ between these two conditions and, crucially, included genes involved in central metabolic processes such as sulfur oxidation, fixation of carbon dioxide (CO_2), energy generation and stress response (Figure S2, Table S3). Because the presence of oxygen, irrespective of its concentration, resulted in a similar metabolic response, we treated the samples derived from hypoxic and oxygen-saturated incubations as biological replicates, and we will hereafter refer to them as the oxic (O) condition.

As such, we consider the AS condition as a proxy for the environment experienced by *Ca*. T. oneisti in deep pore water, and the O condition as the one experienced by the symbiont in superficial pore water. Differential gene expression analysis revealed that 21.7% of all genes exhibited significantly different expression between these two conditions (Figure S2C), and we will present their expression analysis below.

Sulfur oxidation genes are upregulated in anoxia

Ca. T. oneisti genes encoding for a sulfur oxidation pathway similar to that of the related but free-living purple sulfur bacterium *Allochromatium vinosum* were highly expressed in both conditions compared with other central metabolic processes, albeit median gene expression was higher in AS compared with oxic conditions (Figure 1). Consistently, 22 out of the 23 differentially expressed genes involved in sulfur oxidation, were upregulated in anoxia relative to oxic conditions (Figure 2A). These mostly included genes involved in the cytoplasmic branch of sulfur oxidation, i.e. genes associated with sulfur transfer from sulfur storage globules (*rhd, tusA, dsrE2*), genes encoding for the reverse-acting Dsr (dissimilatory sulfite reductase) system involved in the oxidation of stored elemental sulfur (S^0) to sulfite and, finally, also the genes required for further oxidation of sulfite to sulfate in the cytoplasm by two sets of adenylylsulfate (APS) reductase (*aprAB*) and one membrane-binding subunit (*aprM*) [55]. Genes encoding a quinone-interacting membrane-bound oxidoreductase (*qmoABC*) exhibited the same expression pattern. This is noteworthy, as AprM and QmoABC are hypothesized to have an analogous function, and their co-occurrence is rare among sulfur-oxidizing bacteria [55, 56].

Concerning genes involved in the periplasmic branch of sulfur oxidation such as the two types of sulfide-quinone reductases (*sqrA*, *sqrF*; oxidation of sulfide), the Sox system and the thiosulfate dehydrogenase (*tsdA*) both involved in oxidation of thiosulfate, transcript levels were unchanged between both conditions (Data S1). Only the flavoprotein subunit of the periplasmic flavocytochrome c sulfide dehydrogenase (*fccB*) was downregulated in the absence of oxygen (Figure 2A).

To assess whether upregulation of sulfur oxidation genes under anoxia was due to the absence of oxygen or the presence of sulfide, we performed an additional anoxic incubation without providing sulfide. Differential expression analysis between the anoxic conditions with and without sulfide revealed that transcript levels of 92.3% of all expressed genes did not significantly differ (Figure S2C). Importantly, sulfur oxidation genes were

447 similarly upregulated, irrespective of the presence of supplemented sulfide (Figure S3). In
448 addition, proteome data derived from incubations with and without oxygen, but no added
449 sulfide showed that one copy of AprA and AprM were among the top expressed proteins
450 under anoxia (Table S4, Supplementary Materials & Methods). Raman microspectroscopy
451 revealed that not only elemental stored sulfur (S^0) was still available at the end of all
452 incubations but there was no significant difference between the S^0 content of the anoxic (no
453 sulfide added) and O conditions (Figures 2B).

454 Collectively, our data indicate that despite the simultaneous availability of S^0 and
455 oxygen (O condition), anoxia increased the transcription of genes involved in sulfur oxidation
456 to sulfate.

457

458 **Sulfur oxidation is coupled to denitrification**

459 Given that sulfur oxidation was upregulated in anoxia, we expected this process to be
460 coupled to the reduction of anaerobic electron acceptors, and nitrate respiration has been
461 shown for symbiotic *L. oneistus* [20]. Consistently, genes encoding for components of the
462 four specific enzyme complexes active in denitrification (*nap*, *nir*, *nor*, *nos*) as well as two
463 subunits of the respiratory chain complex III (*petA* and *petB* of the cytochrome bc1 complex,
464 which is known for being involved in denitrification and in the aerobic respiratory chain; [57])
465 were upregulated under anoxia (Figures 2A and S4).

466 In accordance with the upregulation of both sulfur oxidation and denitrification genes
467 we observed via RNA-Seq, RT-qPCR targeting *aprA*, *dsrA* and *norB* transcripts showed that
468 these genes were significantly higher expressed under anoxia in the closely related
469 ectosymbiont of *Catanema* sp., which possesses the same central metabolic capabilities as
470 *Ca.* T. oneisti ([11]; Supplementary Materials & Methods, Figures S5 and S6).

471 Besides nitrate respiration, *Ca*. T. oneisti may also be capable of utilizing dimethyl
472 sulfoxide (DMSO) as a terminal electron acceptor since we observed an upregulation of all
473 three subunits of a putative DMSO reductase (*dmsABC* genes). Concerning other electron
474 acceptors, the symbiont has the genetic potential to carry out fumarate reduction (*frd* genes,

475 Data S1), and we identified a potential rhodoquinone biosynthesis gene (*rquA*), which acts
476 as anaerobic electron carrier involved in fumarate reduction in only a few prokaryotic and
477 eukaryotic organisms [58, 59]. Its upregulation under anoxic conditions indeed suggests an
478 active role in anaerobic energy generation in *Ca.* T. oneisti (Figure S4).

479 Intriguingly, lipid profiles of the symbiont revealed a change in lipid composition as
480 well as significantly higher relative abundances of several lyso-phospholipids under anoxia
481 (Figure S7, Supplementary Materials & Methods), possibly resulting in altered uptake
482 behavior and higher membrane permeability for electron donors and acceptors [60–63].
483 Notably, we also detected lyso-phosphatidylcholine to be significantly more abundant in
484 anoxia (Figure S7). As the symbiont does not possess known genes for biosynthesis of this
485 lipid, it may be host-derived. Incorporation of host lipids into symbiont membranes was
486 reported previously [64, 65].

487 Our data support that under anoxia, *Ca*. Thiosymbion gain energy by coupling sulfur
488 oxidation to complete reduction of nitrate to dinitrogen gas. Moreover, the symbiont appears
489 to exploit oxygen-depleted environments for energy generation by utilizing nitrate, DMSO
490 and fumarate as electron acceptors.

491

492 **Sulfur oxidation is decoupled from carbon fixation**

493 Several thioautotrophic symbionts have been shown to utilize the energy generated by sulfur
494 oxidation for fixation of inorganic carbon [6, 66–70]. Previous studies strongly support that
495 *Ca.* T. oneisti is capable of fixing carbon via an energy-efficient Calvin-Benson-Bassham
496 (CBB) cycle [5, 15, 17, 19, 71]. In this study, bulk isotope-ratio mass spectrometry (IRMS)
497 conducted with symbiotic nematodes confirmed that they incorporate ^{13}C-labelled inorganic
498 carbon. Remarkably, however, we detected incorporation of $^{13}CO_2$ under both anoxic and
499 oxic conditions to a similar extent in the course of 24 h (Figure 2C). To localize the sites of
500 $^{13}CO_2$ incorporation, we subjected $^{13}CO_2$-incubated symbiotic nematodes to nanoscale
501 secondary ion mass spectrometry (NanoSIMS) and detected ^{13}C enrichment predominantly
502 within the cells of the symbiont (Figure S8, Supplementary Materials & Methods).

503 Consistent with the evidence for carbon fixation by the ectosymbiont, all genes
504 related to the CBB cycle were detected, both on the transcriptome and the proteome level,
505 with high transcript levels under both anoxic and oxic conditions (Figure 1, Data S1).
506 However, the upregulation of sulfur oxidation genes observed under anoxia did not coincide
507 with an upregulation of carbon fixation genes. On the contrary, the median expression level
508 of all carbon fixation genes was higher in the presence of oxygen (Figure 1). In particular,
509 the transcripts encoding for the small subunit of the key CO_2-fixation enzyme ribulose-1,5-
510 bisphosphate carboxylase/oxygenase RuBisCO (*cbbS*) together with the transcripts
511 encoding its activases (*cbbQ* and *cbbO;* [72]) and the PPi-dependent 6-phosphofructokinase
512 (PPi-PFK; [73, 74]) were significantly more abundant under oxic conditions (Figure 2A).
513 Consistently, the large subunit of the RuBisCO protein (CbbL), which was among the top
514 expressed proteins in both conditions, was slightly more abundant in the presence of oxygen
515 (Table S4).
516 In accordance with our omics data, phylogenetic analysis of the *Ca.* T. oneisti
517 RuBisCO large subunit protein (CbbL) (Figure S9) shows that it clusters within the type I-A
518 group, whose characterized representatives are adapted to higher oxygen concentrations
519 [75].
520 In conclusion, key CO_2 fixation genes are upregulated in the presence of oxygen,
521 albeit inorganic carbon is incorporated to a similar extent under oxic and anoxic conditions.
522 In contrast to what has been reported about other thiotrophic bacteria, the upregulation of
523 sulfur oxidation genes was not accompanied by upregulation of genes involved in CO_2
524 fixation. Therefore, we hypothesize that (1) under anoxia, the energy derived from sulfur
525 oxidation is not completely utilized for carbon fixation and that (2) under oxic conditions
526 another electron donor besides sulfide contributes to energy generation for carbon fixation
527 (see section below).
528
529 **Genes involved in the utilization of organic carbon and PHA storage build-up are**
530 **upregulated under oxic conditions**

531 As anticipated, the nematode ectosymbiont may exploit additional reduced compounds
532 besides sulfide for energy generation. Indeed, *Ca*. T. oneisti possesses the genomic
533 potential to assimilate glyoxylate, acetate and propionate via the partial 3-hydroxypropionate
534 bi-cycle (like the closely related *Olavius algarvensis* γ1 symbiont; [73]), and furthermore
535 encodes genes for utilizing additional organic carbon compounds such as glycerol 3-
536 phosphate, glycolate, ethanol and lactate (Data S1). Figure 1 shows that, overall, the
537 expression of genes involved in the assimilation of organic carbon was higher under oxic
538 conditions. Among the upregulated genes were *lutB* (involved in oxidation of lactate to
539 pyruvate; [76]) and propionyl-CoA synthetase (*prpE,* propanoate assimilation; [77]) (Data
540 S1).

541 These gene expression data imply that the nematode ectosymbiont utilizes organic
542 carbon compounds in addition to CO_2 under oxic conditions, thereby increasing the supply of
543 carbon Consistent with high carbon availability, genes necessary to synthesize storage
544 compounds such as polyhydroxyalkanoates (PHA), glycogen and trehalose showed an
545 overall higher median transcript level under oxic conditions (Figure 1). In particular, two key
546 genes involved in the biosynthesis of the PHA compound polyhydroxybutyrate (PHB) –
547 acetyl-CoA acetyltransferase (*phaA*) and a class III PHA synthase subunit (*phaC*) – were
548 upregulated in the presence of oxygen. Conversely, we observed upregulation of both PHB
549 depolymerases under anoxia, and Raman microspectroscopy showed that significantly less
550 PHA was present in symbionts incubated in anoxia (Figure S10).

551 We propose that under oxic conditions, enhanced mixotrophy (i.e., CBB cycle-
552 mediated carbon fixation and organic carbon utilization) would result in higher carbon
553 availability reflected by PHA storage build-up and facilitating chemoorganoheterotrophic
554 synthesis of ATP via the aerobic respiratory chain.

555

556 **Upregulation of nitrogen assimilation under oxic conditions**

557 It has been shown that high carbon availability is accompanied by high nitrogen assimilation
558 [78–80]. Indeed, despite the sensitivity of nitrogenase towards oxygen [81], its key catalytic

559 MoFe enzymes (*nifD, nifK*; [82]) and several other genes involved in nitrogen fixation were
560 drastically upregulated in the presence of oxygen (Figures 1 and 3). RT-qPCR revealed an
561 increase of *nifH* transcripts also in the ectosymbiont of *Catanema* sp. when oxygen was
562 present (Figure S5, Supplementary Materials & Methods). Moreover, in accordance with a
563 recent study showing the importance of sulfur assimilation for nitrogen fixation [83], genes
564 involved in assimilation of sulfate, i.e. the sulfate transporters *sulP* and *cys*Z as well as
565 genes encoding two enzymes responsible for cysteine biosynthesis (*cysM*, *cysE*) were also
566 upregulated in the presence of oxygen (Data S1).

567 Besides nitrogen fixation, genes involved in urea uptake (transporters, *urtCBDE*) and
568 utilization (urease, *ureF* and *ureG*) were also significantly higher transcribed under oxic
569 conditions (Figures 1 and 3).

570 In conclusion, genes involved in assimilation of nitrogen (N_2 and urea) were
571 consistently upregulated in the presence of oxygen, when (1) carbon assimilation was likely
572 higher, and when (2) higher demand for nitrogen is expected due to stress-induced
573 synthesis of vitamins (see section below).

574

575 **Upregulation of biosynthesis of cofactors and vitamins and global stress response**
576 **under oxic conditions**

577 Multiple transcripts and proteins associated with a diverse bacterial stress response were
578 among the top expressed under oxic conditions (Figure 1 and Table S4). More specifically,
579 heat-shock proteins Hsp70 and Hsp90 were highly abundant (Table S4), and transcripts of
580 heat-shock proteins (Hsp15, Hsp40 and Hsp90) were upregulated (Figure 4A). Besides
581 chaperones, we also detected upregulation of superoxide dismutase (*sodB*), involved in the
582 scavenging of reactive oxygen species (ROS) [84], a transcription factor which induces
583 synthesis of Fe-S clusters under oxidative stress (*iscR*; [85, 86]) along with several other
584 genes involved in Fe-S cluster formation (Figure 4B, [87]), and regulators for redox
585 homeostasis, like thioredoxins, glutaredoxins and peroxiredoxins [88]. Furthermore, we
586 observed upregulation of protease genes (*rseP*, *htpX*, *hspQ*; [89–91]), genes required for

587 repair of double-strand DNA breaks (such as *radA*, *recB* and *mutSY*; [92, 93]) and even
588 genes that are involved in the response to amino acid, iron and fatty acid starvation (*relA*,
589 *spoT*, *sspA*; [94–97]) (Figure 4A).

590 We hypothesized that the drastic upregulation of stress-related genes observed
591 under oxic conditions would entail an increase in biosynthesis of vitamins [98–100]. Indeed,
592 genes involved in biosynthesis of vitamins such as vitamins B_2, B_6, and B_{12} were upregulated
593 under oxic conditions (Figures 1 and 4A). The proposed upregulation of nitrogen fixation and
594 urea utilization would support the synthesis of these nitrogen-rich molecules.

595 The upregulation of stress-related genes under oxic conditions was accompanied by
596 significantly fewer dividing symbiont cells (19.2% under oxic versus 30.1% under anoxic
597 conditions) (Figure 4B) and downregulation of early (*ftsEX*, *zipA*, *zapA*) and late (*damX*,
598 *ftsN*) cell division genes ([101], Figure 1 and Data S1). Oxygen therefore elicits a stress
599 response that affects symbiont proliferation.

600

601 **Discussion**

602 Although transcriptomic analysis was used to study the response of a vent snail
603 endosymbiont to changes in reduced sulfur species [69], up to this study, no thiotrophic
604 ectosymbiont has been subjected to global gene expression profiling under variable
605 environmental conditions. Therefore, our study provides unique insights into the global
606 physiological response of animal-attached bacteria that must thrive in the face of fluctuating
607 concentrations of substrates for energy generation.

608 We performed omics-based gene expression profiling on the nematode ectosymbiont
609 *Ca*. T. oneisti exposed to sulfide and oxygen at concentration levels encountered in its
610 habitat. In particular, the provided sulfide concentrations (< 25 μM) were comparable to
611 those reported for *Stilbonematinae* inhabiting sand areas in which sulfide concentrations
612 gradually increase with depth but are relatively low on average [21]. Given that in these so-
613 called "cool spots" oxygen and sulfide hardly co-occur [102, 103], we did not add any sulfide
614 to oxygenated seawater in our experimental set-up. However, given that stores of elemental

615 sulfur were still detected under all conditions after the incubation period and sulfur oxidation
616 genes were also upregulated in anoxic incubations without added sulfide, the electron donor
617 was available even when sulfide was not supplied, i.e. the ectosymbiont was not starved of
618 electron donor. In this study, we detected a stark transcriptional response of *Ca*.
619 Thiosymbion key metabolic processes to oxygen. The influence of oxygen on physiology
620 was globally reflected also by shifts in protein abundance and lipid composition.
621

622 **Anaerobic sulfur oxidation**

623 Genes involved in sulfur oxidation showed high overall expression compared to other central
624 metabolic processes, indicating that thiotrophy is the predominant energy-generating
625 process for *Ca.* T. oneisti in both oxic and anoxic conditions (Figure 5). Our data thus
626 strongly support previous observations of *Stilbonematinae* ectosymbionts performing aerobic
627 or anaerobic sulfur oxidation [19, 20]. As the majority of genes involved in denitrification
628 were upregulated in anoxia (Figures 2A and 5) and, importantly, we detected nitrate from the
629 most superficial down to the deepest pore water zones (Table S1), nitrate likely serves as
630 terminal electron acceptor for anaerobic sulfur oxidation.

631 Because sulfur oxidation in chemosynthetic symbioses is commonly described as an
632 aerobic process that also suits the host animal's physiology [2], anaerobic sulfur oxidation
633 seems extraordinary. However, many of these symbiotic organisms likely experience periods
634 of oxygen depletion as would be expected from life at the interface of oxidized and reduced
635 marine environments. Early studies on the physiology of a few thiotrophic symbionts indeed
636 describe nitrate reduction in the presence of sulfide under anoxic conditions [24–26].
637 Moreover, genes for nitrate respiration have been found in thiotrophic symbionts of a variety
638 of shallow-water and deep-sea vent animals [5, 73, 104–106]. Utilizing nitrate as an
639 alternative terminal electron acceptor during anaerobic sulfur oxidation to bridge temporary
640 anoxia could thus be a more important strategy for energy conservation among thiotrophic
641 symbionts than currently acknowledged.

Although relevant for organisms exposed to highly fluctuating oxygen concentrations, this is the first study to show differential gene expression of a symbiont's sulfur oxidation pathway between anoxic and oxic conditions. Specifically, the majority of sulfur oxidation genes, and in particular genes encoding the cytoplasmic branch of sulfur oxidation, were strongly upregulated under anoxic conditions (Figure 2). While upregulation of sulfur oxidation and denitrification genes under anoxia represents no proof for preferential anaerobic sulfur oxidation, we hypothesize that oxidation of reduced sulfur compounds to sulfate is more pronounced under anoxia.

Among the upregulated sulfur oxidation genes, we identified *aprM* and the *qmoABC* complex, both of which are thought to act as electron-accepting units for APS reductase, and therefore rarely co-occur in thiotrophic bacteria [55]. The presence and expression of the QmoABC complex could provide a substantial energetic advantage to the ectosymbiont by mediating electron bifurcation [55], in which the additional reduction of a low-potential electron acceptor (e.g. ferredoxin, NAD^+) could result in optimized energy conservation under anoxic conditions. The maximization of sulfur oxidation under anoxia might even represent a temporary advantage for the host, as it would protect the animal from sulfide poisoning while crawling in predator-free and detritus-rich sand [20, 107–109]. Due to the dispensability of oxygen for sulfur oxidation, the ectosymbiont may not need to be shuttled to superficial sand by their nematode hosts to oxidize sulfur. Host migration into upper zones of the sediment may therefore primarily reflect the animal's aerobic physiology.

In addition to anaerobic sulfur oxidation, the nematode ectosymbiont's phylogenetic affiliation with anaerobic, phototrophic sulfur oxidizers such as *Allochromatium vinosum* [5, 110], and also the presence and expression of yet other anaerobic respiratory complexes (DMSO and fumarate reductase) collectively suggest that *Ca*. Thiosymbion is well-adapted to anoxic, sulfidic sediment zones.

Symbiont proliferation in anoxia

669 Pivotal studies addressed the extraordinary strategies *Ca*. T. oneisti evolved to grow and
670 divide [12, 14, 111]; yet, due to the difficulty in cultivation, the physiological basis of
671 longitudinal cell division has never been addressed.

672 In this study, significantly higher numbers of dividing cells were found under AS
673 conditions (Figure 4B, Data S1) and therefore, sulfur oxidation coupled to denitrification
674 might represent the ectosymbiont's preferred metabolism for growth. We hypothesize that
675 aside from sulfur oxidation, the mobilization of PHA could represent an additional source of
676 ATP (and carbon) supporting symbiont proliferation under anoxia (Figure S10, Figure 5). Of
677 note, PHA mobilization in anoxia was also shown for *Beggiatoa* spp. [112]. Furthermore,
678 several lines of research have shown that stress can inhibit growth in bacteria [113–119].
679 Importantly, studies on growth preferences of thiotrophic symbionts are lacking, and
680 proliferation of a thiotroph with anaerobic electron acceptors (such as nitrate) has never
681 been observed before [120–123].

682

683 **Decoupling of sulfur oxidation from carbon fixation**

684 A series of evidences gained by experiments conducted in the presence of oxygen indicate
685 that several thioautotrophic symbionts fuel carbon fixation by sulfur oxidation-generated
686 energy [6, 66–70]. Furthermore, (1) the giant tube worm *Riftia pachyptila* was recently
687 shown to exhibit higher inorganic carbon incorporation rates when incubated with sulfide and
688 high oxygen concentrations [124], (2) carbon fixation by the clam *Solemya velum* symbiont
689 was stimulated by sulfide and oxygen but not when nitrate was supplied as electron acceptor
690 [125] and (3) Schiemer *et al*. [19] showed that sulfide supported the uptake of CO_2 in
691 symbiotic nematodes incubated in the presence of oxygen. Although our bulk isotope-ratio
692 mass spectrometry (IRMS) and transcriptomic analyses indicate carbon fixation under both
693 anoxic and oxic conditions, the mere presence of sulfide did not appear to stimulate
694 incorporation of inorganic carbon. Instead, key carbon fixation genes of *Ca*. T. oneisti were
695 upregulated when oxygen was present (Figure 2). Therefore, carbon fixation appears to be
696 decoupled from anaerobic sulfur oxidation, and to rely on oxygen more than previously

697 acknowledged. An example of extreme decoupling of sulfur oxidation and carbon fixation
698 was recently reported for *Kentrophoros* ectosymbionts, which were shown to lack genes for
699 autotrophic carbon fixation altogether and thus represent the first heterotrophic sulfur-
700 oxidizing symbionts [71].

701 Finally, regarding the fate of the fixed carbon, symbiont biomass build-up does not
702 seem to solely rely on autotrophically-derived organic carbon, as the symbiont appeared to
703 proliferate more in anoxia, when expression of carbon fixation genes was lower. Conversely,
704 CO_2 fixed under oxic conditions may not be exclusively used for biomass generation (Figure
705 5).

706

707 **Oxic mixotrophy**

708 Besides chemoautotrophy, several chemosynthetic symbionts may engage in mixotrophy [5,
709 69, 73, 74, 126]. Also the nematode ectosymbiont possesses genes involved in the
710 assimilation of organic carbon such as lactate, propionate, acetate and glycolate, and their
711 expression was more pronounced under oxic conditions (Figure 1). Additional indications for
712 mixotrophy comprise the presence and expression of genes for several transporters for
713 small organic carbon compounds, a pyruvate dehydrogenase complex (*aceE, aceF, lpd*),
714 and a complete TCA cycle, including a 2-oxoglutarate dehydrogenase (*korA*, *korB*), which is
715 often lacking in obligate autotrophs [127] (Data S1). The ectosymbiont thus appears to
716 assimilate both inorganic and organic carbon under oxic conditions and may consequently
717 experience higher carbon availability (Figure 5).

718 The metabolization of these carbon compounds ultimately yields acetyl-CoA, which
719 in turn could be further oxidized in the TCA cycle and/or utilized for fatty acid and PHA
720 biosynthesis. Our transcriptome and Raman microspectroscopy data suggest that *Ca*. T.
721 oneisti favors PHA build-up over degradation under oxic conditions. Thus, PHA
722 accumulation in the presence of oxygen can be explained by higher carbon availability. In
723 addition, it might play a role in resilience against cellular stress, as there is increasing
724 evidence that PHA biosynthesis is enhanced under unfavorable growth conditions such as

extreme temperatures, UV radiation, osmotic shock and oxidative stress [128–136]. Similar findings have been obtained for pathogenic [137] and symbiotic bacteria of the genus *Burkholderia* [138]; the latter study reports upregulation of stress response genes and PHA biosynthesis in the presence of oxygen. Finally, oxic biosynthesis of PHA might also prevent excessive accumulation and breakdown of sugars by glycolysis and oxidative phosphorylation, which, in turn, would exacerbate oxidative stress [139].

Oxic nitrogen assimilation

Despite the oxygen-sensitive nature of nitrogenase [81], we observed a drastic upregulation of nitrogen fixation genes (Figures 1 and 3). In addition, urea utilization and uptake genes were also upregulated. Although the nematode host likely lacks the urea biosynthetic pathway (L.K., unpublished data), this compound is one of the most abundant organic nitrogen substrates in marine ecosystems, as well as in animal-inhabited oxygenated sand layers [140, 141]. Notably, the upregulation of the urea uptake system and urease accessory proteins has been shown to be a response to nitrogen limitation in other systems [142].

An alternative or additional explanation for the apparent increase in nitrogen assimilation in the presence of oxygen could be the need to synthesize nitrogen-rich compounds such as vitamins and cofactors to survive oxidative stress (Figures 1 and 4). The role of vitamins in protecting cells against the deleterious effects of oxygen has been shown for animals [143, 144], and the importance of riboflavin for bacterial survival under oxidative stress has previously been reported [98, 100]. Along this line of thought, oxygen-exposed *Ca.* T. oneisti upregulated glutathione and thioredoxin, which are known to play a pivotal role in scavenging reactive oxygen species (ROS) [145]. Their function directly (or indirectly) requires vitamin B_2, B_6 and B_{12} as cofactors. More specifically, thioredoxin reductase (*trxB*) requires riboflavin (vitamin B_2) in the form of flavin adenine dinucleotide (FAD) [146]; cysteine synthase (*cysM*) and glutamate synthases (two-subunit *gltB*/*gltD,* one-subunit *gltS*) involved in the biosynthesis of the glutathione precursors L-cysteine and L-glutamate depend on vitamin B_6, FAD and riboflavin in the form of flavin mononucleotide

(FMN) [147, 148]. As for cobalamin, it was thought that this vitamin only played an indirect role in oxidative stress resistance [149], by being a precursor of S-adenosyl methionine (SAM), a substrate involved in the synthesis of glutathione via the methionine metabolism (and the transulfuration pathway), and in preventing the Fenton reaction [150, 151]. However, its direct involvement in the protection of chemolithoautotrophic bacteria against oxidative stress has also been illustrated [99].

In summary, in the presence of oxygen, the upregulation of genes involved in biosynthesis of vitamins B_2, B_6 and B_{12} along with antioxidant systems and their key precursor genes *cysM*, *gltD* and B_{12}-dependent-methionine synthase *metH*, suggests that the ectosymbiont requires increased levels of these vitamins to cope with oxidative stress (Figure 5).

Evolutionary considerations

Anaerobic sulfur oxidation, increased symbiont proliferation and downregulation of stress-related genes lead us to hypothesize that *Ca.* T. oneisti evolved from a free-living bacterium that mostly, if not exclusively, inhabited anoxic sand zones. In support of this, the closest relatives of the nematode ectosymbionts are free-living obligate anaerobes from the family *Chromatiaceae* (i.e. *Allochromatium vinosum*, *Thioflavicoccus mobilis*, *Marichromatium purpuratum*) [5, 152]. Eventually, advantages such as protection from predators or utilization of host waste products (e.g. fermentation products, ammonia) may have been driving forces that led to the *Ca*. Thiosymbion-*Stilbonematinae* symbioses. As the association became more and more stable, the symbiont optimized (or acquired) mechanisms to resist oxidative stress, as well as metabolic pathways to most efficiently exploit the metabolic potential of oxygenated sand zones (mixotrophy, nitrogen assimilation, vitamin and cofactor biosynthesis). From the viewpoint of the host, the acquired “symbiotic skin” enabled *L. oneistus* to tolerate the otherwise poisonous sulfide and thrive in sand layers virtually devoid of predators and rich in decomposed organic matter (detritus).

Acknowledgements

This work was supported by the Austrian Science Fund (FWF) grant P28743 (T. V., S. B. and L. K.) and the DK plus: Microbial Nitrogen Cycling (G. F. P.). We are indebted to the staff of the VBCF NGS Unit (Laura-Maria Bayer and Miriam Schalamun) for assistance with Oxford Nanopore MinION sequencing and to Florian Goldenberg, Patrick Hyden and Thomas Rattei (Division of Computational Systems Biology, University of Vienna) for providing and maintaining the Life Science Compute Cluster (LiSC) and help in preparing the MinION sequencing library for *Ca.* T. oneisti at the University of Vienna. Harald Gruber-Vodicka from the MPI Bremen generously provided Illumina raw reads to aid the assemblies of ectosymbiont genomes. We are very grateful to Wiebke Mohr, Nikolaus Leisch and Nicole Dubilier from the MPI for Marine Microbiology (Bremen) for continuous technical support with the stable isotope-based techniques and anaerobic atmosbag and Andreas Maier for DOC measurements (data not shown). We thank Olivier Gros from the Université des Antilles for making all the experiments involving *Catanema sp.* possible. We appreciate Tjorven Hinzke's advice on metaproteome statistics and Carolina Reyes for her input on the nitrogen metabolism. We thank Yin Chen for providing the facilities for lipidomic analysis and Eleonora Silvano for assistance with lipid extractions, and Jana Matulla's and Sebastian Grund's excellent technical work during protein sample preparation and MS analysis, respectively. Also, our sincere gratitude to the Carrie Bow Cay Laboratory, Caribbean Coral Reef Ecosystem Program and his Station Manager Zach Foltz for his help during field work. Finally, we were very much helped and inspired by insightful discussions with Monika Bright, Jörg A. Ott, Christa Schleper, Simon Rittmann, Filipa Sousa and Jillian Petersen.

Competing Interests

The authors declare no competing financial interest.

References

1. Ott J, Bright M, Bulgheresi S. Marine microbial thiotrophic ectosymbioses. In: Gibson RN, Atkinson RJA, Gordon JDM (eds). *Oceanography and Marine Biology: An Annual Review*, 42nd ed. 2004. pp 95–118.
2. Dubilier N, Bergin C, Lott C. Symbiotic diversity in marine animals: the art of harnessing chemosynthesis. *Nat Rev Microbiol* 2008; **6**: 725–740.
3. Stewart FJ, Newton ILG, Cavanaugh CM. Chemosynthetic endosymbioses: adaptations to oxic–anoxic interfaces. *Trends Microbiol* 2005; **13**: 439–448.
4. König S, Gros O, Heiden SE, Hinzke T, Thürmer A, Poehlein A, et al. Nitrogen fixation in a chemoautotrophic lucinid symbiosis. *Nat Microbiol* 2016; **2**: 16193.
5. Petersen JM, Kemper A, Gruber-Vodicka H, Cardini U, van der Geest M, Kleiner M, et al. Chemosynthetic symbionts of marine invertebrate animals are capable of nitrogen fixation. *Nat Microbiol* 2016; **2**: 16195.
6. Ponsard J, Cambon-Bonavita M-A, Zbinden M, Lepoint G, Joassin A, Corbari L, et al. Inorganic carbon fixation by chemosynthetic ectosymbionts and nutritional transfers to the hydrothermal vent host-shrimp *Rimicaris exoculata*. *ISME J* 2013; **7**: 96–109.
7. Polz MF, Distel DL, Zarda B, Amann R, Felbeck H, Ott JA, et al. Phylogenetic analysis of a highly specific association between ectosymbiotic, sulfur-oxidizing bacteria and a marine nematode. *Appl Environ Microbiol* 1994; **60**: 4461–4467.
8. Bayer C, Heindl NR, Rinke C, Lücker S, Ott J, Bulgheresi S. Molecular characterization of the symbionts associated with marine nematodes of the genus *Robbea*. *Environ Microbiol Rep* 2009; **1**: 136–144.
9. Williams KP, Gillespie JJ, Sobral BWS, Nordberg EK, Snyder EE, Shallom JM, et al. Phylogeny of gammaproteobacteria. *J Bacteriol* 2010; **192**: 2305–2314.
10. Pende N, Leisch N, Gruber-Vodicka HR, Heindl NR, Ott J, den Blaauwen T, et al. Size-independent symmetric division in extraordinarily long cells. *Nat Commun* 2014; **5**: 4803.
11. Zimmermann J, Wentrup C, Sadowski M, Blazejak A, Gruber-Vodicka HR, Kleiner M,

et al. Closely coupled evolutionary history of ecto- and endosymbionts from two distantly related animal phyla. *Mol Ecol* 2016; **25**: 3203–3223.

12. Leisch N, Verheul J, Heindl NR, Gruber-Vodicka HR, Pende N, den Blaauwen T, et al. Growth in width and FtsZ ring longitudinal positioning in a gammaproteobacterial symbiont. *Curr Biol* 2012; **22**: R831–R832.

13. Leisch N, Pende N, Weber PM, Gruber-Vodicka HR, Verheul J, Vischer NOE, et al. Asynchronous division by non-ring FtsZ in the gammaproteobacterial symbiont of *Robbea hypermnestra*. *Nat Microbiol* 2016; **2**: 1–5.

14. Pende N, Wang J, Weber PM, Verheul J, Kuru E, Rittmann SK-MR, et al. Host-polarized cell growth in animal symbionts. *Curr Biol* 2018; **28**: 1039-1051.e5.

15. Ott JA, Novak R, Schiemer F, Hentschel U, Nebelsick M, Polz M. Tackling the sulfide gradient: a novel strategy involving marine nematodes and chemoautotrophic ectosymbionts. *Mar Ecol* 1991; **12**: 261–279.

16. Powell EN, Crenshaw MA, Rieger RM. Adaptations to sulfide in the meiofauna of the sulfide system. I. 35S-sulfide accumulation and the presence of a sulfide detoxification system. *J Exp Mar Bio Ecol* 1979; **37**: 57–76.

17. Polz MF, Felbeck H, Novak R, Nebelsick M, Ott JA. Chemoautotrophic, sulfur-oxidizing symbiotic bacteria on marine nematodes: morphological and biochemical characterization. *Microb Ecol* 1992; **24**: 313–329.

18. Himmel D, Maurin LC, Gros O, Mansot J-L. Raman microspectrometry sulfur detection and characterization in the marine ectosymbiotic nematode *Eubostrichus dianae* (Desmodoridae, Stilbonematidae). *Biol Cell* 2009; **101**: 43–54.

19. Schiemer F, Novak R, Ott J. Metabolic studies on thiobiotic free-living nematodes and their symbiotic microorganisms. *Mar Biol* 1990; **106**: 129–137.

20. Hentschel U, Berger E, Bright M, Felbeck H, Ott J. Metabolism of nitrogen and sulfur in ectosymbiotic bacteria of marine nematodes (Nematoda, Stilbonematinae). *Mar Ecol Prog Ser* 1999; **183**: 149–158.

21. Ott J, Novak R. Living at an interface: Meiofauna at the oxygen/sulfide boundary in

marine sediments. In: Ryland JS, Tyler PA (eds). *Reproduction, Genetics and Distributions of Marine Organisms*. 1989. Olsen & Olsen, Fredensborg, pp 415–422.

22. Canfield DE, Thamdrup B. Towards a consistent classification scheme for geochemical environments, or, why we wish the term 'suboxic' would go away. *Geobiology* 2009; **7**: 385–392.

23. Luther GW, Findlay AJ, MacDonald DJ, Owings SM, Hanson TE, Beinart RA, et al. Thermodynamics and kinetics of sulfide oxidation by oxygen: a look at inorganically controlled reactions and biologically mediated processes in the environment. *Front Microbiol* 2011; **2**: 62.

24. Wilmot DB, Vetter RD. Oxygen- and nitrogen-dependent sulfur metabolism in the thiotrophic clam *Solemya reidi*. *Biol Bull* 1992; **182**: 444–453.

25. Hentschel U, Cary SC, Felbeck H. Nitrate respiration in chemoautotrophic symbionts of the bivalve *Lucinoma aequizonata*. *Mar Ecol Prog Ser* . 1993. Inter-Research Science Center. , **94**: 35–41

26. Hentschel U, Felbeck H. Nitrate respiration in the hydrothermal vent tubeworm *Riftia pachyptila*. *Nature* 1993; **366**: 338–340.

27. Cline JD. Spectrophotometric determination of hydrogen sulfide in natural waters. *Limnol Oceanogr* 1969; **14**: 454–458.

28. Green LC, Wagner DA, Glogowski J, Skipper PL, Wishnok JS, Tannenbaum SR. Analysis of nitrate, nitrite, and [15N]nitrate in biological fluids. *Anal Biochem* 1982; **126**: 131–138.

29. Schnetger B, Lehners C. Determination of nitrate plus nitrite in small volume marine water samples using vanadium(III)chloride as a reduction agent. *Mar Chem* 2014; **160**: 91–98.

30. Solórzano L. Determination of ammonia in natural waters by the phenolhypochlorite method. *Limnol Oceanogr* 1969; **14**: 799–801.

31. Kester DR, Duedall IW, Connors DN, Pytkowicz RM. Preparation of artificial seawater. *Limnol Oceanogr* 1967; **12**: 176–179.

32. Alberti A, Belser C, Engelen S, Bertrand L, Orvain C, Brinas L, et al. Comparison of library preparation methods reveals their impact on interpretation of metatranscriptomic data. *BMC Genomics* 2014; **15**: 912.

33. Li H, Durbin R. Fast and accurate short read alignment with Burrows-Wheeler transform. *Bioinformatics* 2009; **25**: 1754–1760.

34. Bankevich A, Nurk S, Antipov D, Gurevich AA, Dvorkin M, Kulikov AS, et al. SPAdes: a new genome assembly algorithm and its applications to single-cell sequencing. *J Comput Biol* 2012; **19**: 455–477.

35. Parks DH, Imelfort M, Skennerton CT, Hugenholtz P, Tyson GW. CheckM: assessing the quality of microbial genomes recovered from isolates, single cells, and metagenomes. *Genome Res* 2015; **25**: 1043–1055.

36. Vallenet D, Calteau A, Dubois M, Amours P, Bazin A, Beuvin M, et al. MicroScope: an integrated platform for the annotation and exploration of microbial gene functions through genomic, pangenomic and metabolic comparative analysis. *Nucleic Acids Res* 2019; **48**: D579–D589.

37. Kanehisa M, Sato Y, Kawashima M, Furumichi M, Tanabe M. KEGG as a reference resource for gene and protein annotation. *Nucleic Acids Res* 2016; **44**: D457–D462.

38. Götz S, Garcia-Gomez JM, Terol J, Williams TD, Nagaraj SH, Nueda MJ, et al. High-throughput functional annotation and data mining with the Blast2GO suite. *Nucleic Acids Res* 2008; **36**: 3420–3435.

39. Bateman A. The Pfam protein families database. *Nucleic Acids Res* 2002; **30**: 276–280.

40. Finn RD, Clements J, Eddy SR. HMMER web server: interactive sequence similarity searching. *Nucleic Acids Res* 2011; **39**: W29–W37.

41. Andrews S. FastQC: a quality control tool for high throughput sequence data. 2010.

42. Schmieder R, Edwards R. Quality control and preprocessing of metagenomic datasets. *Bioinformatics* 2011; **27**: 863–864.

43. Bolger AM, Lohse M, Usadel B. Trimmomatic: a flexible trimmer for Illumina sequence

data. *Bioinformatics* 2014; **30**: 2114–2120.

44. König L, Siegl A, Penz T, Haider S, Wentrup C, Polzin J, et al. Biphasic Metabolism and Host Interaction of a Chlamydial Symbiont. *mSystems* 2017; **2**: e00202-16.

45. Li H, Handsaker B, Wysoker A, Fennell T, Ruan J, Homer N, et al. The sequence alignment/map format and SAMtools. *Bioinformatics* 2009; **25**: 2078–2079.

46. Anders S, Pyl PT, Huber W. HTSeq - A Python framework to work with high-throughput sequencing data. *Bioinformatics* 2014; **31**: 166–169.

47. Gentleman RC, Carey VJ, Bates DM, Bolstad B, Dettling M, Dudoit S, et al. Bioconductor: open software development for computational biology and bioinformatics. *Genome Biol* 2004; **5**: R80.

48. Robinson MD, McCarthy DJ, Smyth GK. edgeR: a Bioconductor package for differential expression analysis of digital gene expression data. *Bioinformatics* 2010; **26**: 139–140.

49. R Development Core Team. R: a language and environment for statistical computing. *R Found Stat Comput* . 2011. R Foundation for Statistical Computing. , **1**: 409

50. Rapaport F, Khanin R, Liang Y, Pirun M, Krek A, Zumbo P, et al. Comprehensive evaluation of differential gene expression analysis methods for RNA-seq data. *Genome Biol* 2013; **14**: R95.

51. Trump BF, Ericsson JL. The effect of the fixative solution on the ultrastructure of cells and tissues. A comparative analysis with particular attention to the proximal convoluted tubule of the rat kidney. *Lab Investig* 1965; **14**: 1245–1323.

52. Samek O, Obruča S, Šiler M, Sedláček P, Benešová P, Kučera D, et al. Quantitative Raman spectroscopy analysis of polyhydroxyalkanoates produced by *Cupriavidus necator* H16. *Sensors* 2016; **16**: 1808.

53. Koppelman C-M, Aarsman MEG, Postmus J, Pas E, Muijsers AO, Scheffers D-J, et al. R174 of <I>Escherichia coli</i> FtsZ is involved in membrane interaction and protofilament bundling, and is essential for cell division. *Mol Microbiol* 2004; **51**: 645–657.

54. Schneider CA, Rasband WS, Eliceiri KW. NIH Image to ImageJ: 25 years of image analysis. *Nat Methods* 2012; **9**: 671–675.

55. Dahl C. Sulfur Metabolism in Phototrophic Bacteria. *Modern Topics in the Phototrophic Prokaryotes*. 2017. Springer International Publishing, Cham, pp 27–66.

56. Ghosh W, Dam B. Biochemistry and molecular biology of lithotrophic sulfur oxidation by taxonomically and ecologically diverse bacteria and archaea. *FEMS Microbiol Rev* 2009; **33**: 999–1043.

57. Chen J, Strous M. Denitrification and aerobic respiration, hybrid electron transport chains and co-evolution. *Biochim Biophys Acta - Bioenerg* 2013; **1827**: 136–144.

58. Lonjers ZT, Dickson EL, Chu T-PT, Kreutz JE, Neacsu FA, Anders KR, et al. Identification of a new gene required for the biosynthesis of rhodoquinone in *Rhodospirillum rubrum*. *J Bacteriol* 2012; **194**: 965–971.

59. Stairs CW, Eme L, Muñoz-Gómez SA, Cohen A, Dellaire G, Shepherd JN, et al. Microbial eukaryotes have adapted to hypoxia by horizontal acquisitions of a gene involved in rhodoquinone biosynthesis. *Elife* 2018; **7**: e34292.

60. Mills JK, Needham D. Lysolipid incorporation in dipalmitoylphosphatidylcholine bilayer membranes enhances the ion permeability and drug release rates at the membrane phase transition. *Biochim Biophys Acta - Biomembr* 2005; **1716**: 77–96.

61. Arouri A, Mouritsen OG. Membrane-perturbing effect of fatty acids and lysolipids. *Prog Lipid Res* . 2013. Pergamon. , **52**: 130–140

62. Koshy C, Schweikhard ES, Gärtner RM, Perez C, Yildiz Ö, Ziegler C. Structural evidence for functional lipid interactions in the betaine transporter BetP. *EMBO J* 2013; **32**: 3096–3105.

63. Laganowsky A, Reading E, Allison TM, Ulmschneider MB, Degiacomi MT, Baldwin AJ, et al. Membrane proteins bind lipids selectively to modulate their structure and function. *Nature* 2014; **510**: 172–175.

64. Wier AM, Nyholm S V, Mandel MJ, Massengo-Tiassé RP, Schaefer AL, Koroleva I, et al. Transcriptional patterns in both host and bacterium underlie a daily rhythm of

anatomical and metabolic change in a beneficial symbiosis. *Proc Natl Acad Sci U S A* 2010; **107**: 2259–64.

65. Saito HE, Harp JR, Fozo EM. Incorporation of exogenous fatty acids protects *Enterococcus faecalis* from membrane-damaging agents. *Appl Environ Microbiol* 2014; **80**: 6527–6538.

66. Cavanaugh CM. Symbiotic chemoautotrophic bacteria in marine invertebrates from sulphide-rich habitats. *Nature* 1983; **302**: 58–61.

67. Nelson DC, Hagen KD, Edwards DB. The gill symbiont of the hydrothermal vent mussel *Bathymodiolus thermophilus* is a psychrophilic, chemoautotrophic, sulfur bacterium. *Mar Biol* 1995; **121**: 487–495.

68. Markert S, Arndt C, Felbeck H, Becher D, Sievert SM, Hügler M, et al. Physiological proteomics of the uncultured endosymbiont of Riftia pachyptila. *Science* 2007; **315**: 247–250.

69. Seston SL, Beinart RA, Sarode N, Shockey AC, Ranjan P, Ganesh S, et al. Metatranscriptional response of chemoautotrophic *Ifremeria nautilei* endosymbionts to differing sulfur regimes. *Front Microbiol* 2016; **7**: 1074.

70. Volland J-M, Schintlmeister A, Zambalos H, Reipert S, Mozetič P, Espada-Hinojosa S, et al. NanoSIMS and tissue autoradiography reveal symbiont carbon fixation and organic carbon transfer to giant ciliate host. *ISME J* 2018; **12**: 714–727.

71. Seah BKB, Antony CP, Huettel B, Zarzycki J, Schada von Borzyskowski L, Erb TJ, et al. Sulfur-oxidizing symbionts without canonical genes for autotrophic CO2 fixation. *MBio* 2019; **10**: e01112-19.

72. Tsai YCC, Lapina MC, Bhushan S, Mueller-Cajar O. Identification and characterization of multiple rubisco activases in chemoautotrophic bacteria. *Nat Commun* 2015; **6**: 8883.

73. Kleiner M, Wentrup C, Lott C, Teeling H, Wetzel S, Young J, et al. Metaproteomics of a gutless marine worm and its symbiotic microbial community reveal unusual pathways for carbon and energy use. *Proc Natl Acad Sci U S A* 2012; **109**: E1173–

E1182.

74. Jäckle O, Seah BKB, Tietjen M, Leisch N, Liebeke M, Kleiner M, et al. Chemosynthetic symbiont with a drastically reduced genome serves as primary energy storage in the marine flatworm *Paracatenula*. *Proc Natl Acad Sci U S A* 2019; **116**: 8505–8514.

75. Tabita FR, Satagopan S, Hanson TE, Kreel NE, Scott SS. Distinct form I, II, III, and IV Rubisco proteins from the three kingdoms of life provide clues about Rubisco evolution and structure/function relationships. *J Exp Bot* 2007; **59**: 1515–1524.

76. Chai Y, Kolter R, Losick R. A widely conserved gene cluster required for lactate utilization in *Bacillus subtilis* and its involvement in biofilm formation. *J Bacteriol* 2009; **191**: 2423–2430.

77. Horswill AR, Escalante-Semerena JC. The prpE gene of *Salmonella typhimurium* LT2 encodes propionyl-CoA synthetase. *Microbiology* 1999; **145**: 1381–1388.

78. Rogers A, Gibon Y, Stitt M, Morgan PB, Bernacchi CJ, Ort DR, et al. Increased C availability at elevated carbon dioxide concentration improves N assimilation in a legume. *Plant, Cell Environ* 2006; **29**: 1651–1658.

79. Elgharably A, Marschner P. Microbial activity and biomass and N and P availability in a saline sandy loam amended with inorganic N and lupin residues. *Eur J Soil Biol* 2011; **47**: 310–315.

80. Fellbaum CR, Gachomo EW, Beesetty Y, Choudhari S, Strahan GD, Pfeffer PE, et al. Carbon availability triggers fungal nitrogen uptake and transport in arbuscular mycorrhizal symbiosis. *Proc Natl Acad Sci* 2012; **109**: 2666–2671.

81. Hill S. How is nitrogenase regulated by oxygen? *FEMS Microbiol Lett* 1988; **54**: 111–129.

82. Burgess BK, Lowe DJ. Mechanism of molybdenum nitrogenase. *Chem Rev* 1996; **96**: 2983–3012.

83. Schneider S, Schintlmeister A, Becana M, Wagner M, Woebken D, Wienkoop S. Sulfate is transported at significant rates through the symbiosome membrane and is

crucial for nitrogenase biosynthesis. *Plant Cell Environ* 2019; **42**: 1180–1189.

84. Hassan HM. Determination of microbial damage caused by oxygen free radicals, and the protective role of superoxide dismutase. *Methods Enzymol* 1984; **105**: 404–412.

85. Schwartz CJ, Giel JL, Patschkowski T, Luther C, Ruzicka FJ, Beinert H, et al. IscR, an Fe-S cluster-containing transcription factor, represses expression of *Escherichia coli* genes encoding Fe-S cluster assembly proteins. *Proc Natl Acad Sci U S A* 2001; **98**: 14895–14900.

86. Yeo W-S, Lee J-H, Lee K-C, Roe J-H. IscR acts as an activator in response to oxidative stress for the *suf* operon encoding Fe-S assembly proteins. *Mol Microbiol* 2006; **61**: 206–218.

87. Zeller T, Moskvin O V., Li K, Klug G, Gomelsky M. Transcriptome and physiological responses to hydrogen peroxide of the facultatively phototrophic bacterium Rhodobacter sphaeroides. *J Bacteriol* 2005; **187**: 7232–7242.

88. Grant CM. Role of the glutathione/glutaredoxin and thioredoxin systems in yeast growth and response to stress conditions. *Mol Microbiol* 2001; **39**: 533–541.

89. Alba BM, Leeds JA, Onufryk C, Lu CZ, Gross CA. DegS and YaeL participate sequentially in the cleavage of RseA to activate the sigma E-dependent extracytoplasmic stress response. *Genes Dev* 2002; **16**: 2156–2168.

90. Sakoh M, Ito K, Akiyama Y. Proteolytic activity of HtpX, a membrane-bound and stress-controlled protease from *Escherichia coli*. *J Biol Chem* 2005; **280**: 33305–33310.

91. Puri N, Karzai AW. HspQ functions as a unique specificity-enhancing factor for the AAA+ Lon protease. *Mol Cell* 2017; **66**: 672-683.e4.

92. Sargentini NJ, Smith KC. Quantitation of the involvement of the *recA*, *recB*, *recC*, *recF*, *recJ*, *recN*, *lexA*, *radA*, *radB*, *uvrD*, and *umuC* genes in the repair of X-ray-induced DNA double-strand breaks in <i>Es. *Radiat Res* 1986; **107**: 58–72.

93. Au KG, Cabrera M, Miller JH, Modrich P. *Escherichia coli mutY* gene product is required for specific A-G----C.G mismatch correction. *Proc Natl Acad Sci* 1988; **85**:

9163–9166.

94. Hansen A-M, Qiu Y, Yeh N, Blattner FR, Durfee T, Jin DJ. SspA is required for acid resistance in stationary phase by downregulation of H-NS in *Escherichia coli*. *Mol Microbiol* 2005; **56**: 719–734.

95. Battesti A, Bouveret E. Acyl carrier protein/SpoT interaction, the switch linking SpoT-dependent stress response to fatty acid metabolism. *Mol Microbiol* 2006; **62**: 1048–1063.

96. Traxler MF, Summers SM, Nguyen H-T, Zacharia VM, Hightower GA, Smith JT, et al. The global, ppGpp-mediated stringent response to amino acid starvation in *Escherichia coli*. *Mol Microbiol* 2008; **68**: 1128–1148.

97. Nguyen D, Joshi-Datar A, Lepine F, Bauerle E, Olakanmi O, Beer K, et al. Active starvation responses mediate antibiotic tolerance in biofilms and nutrient-limited bacteria. *Science (80-)* 2011; **334**: 982–986.

98. Chen J, Shen J, Solem C, Jensen PR. Oxidative stress at high temperatures in Lactococcus lactis due to an insufficient supply of riboflavin. *Appl Environ Microbiol* 2013; **79**: 6140–6147.

99. Ferrer A, Rivera J, Zapata C, Norambuena J, Sandoval Á, Chávez R, et al. Cobalamin protection against oxidative stress in the acidophilic iron-oxidizing bacterium *Leptospirillum* group II CF-1. *Front Microbiol* 2016; **7**: 748.

100. Showman AC, Aranjuez G, Adams PP, Jewett MW. Gene bb0318 is critical for the oxidative stress response and infectivity of *Borrelia burgdorferi*. *Infect Immun* 2016; **84**: 3141–3151.

101. Typas A, Banzhaf M, Gross CA, Vollmer W. From the regulation of peptidoglycan synthesis to bacterial growth and morphology. *Nat Rev Microbiol* 2012; **10**: 123–136.

102. Meyers M, Fossing H, Powell E. Microdistribution of interstitial meiofauna, oxygen and sulfide gradients, and the tubes of macro-infauna. *Mar Ecol Prog Ser* 1987; **35**: 223–241.

103. Powell E. Oxygen, sulfide and diffusion: Why thiobiotic meiofauna must be sulfide-

insensitive first-order respirers. *J Mar Res* 1989; **47**: 887–932.

104. Jan C, Petersen JM, Werner J, Teeling H, Huang S, Glöckner FO, et al. The gill chamber epibiosis of deep-sea shrimp *Rimicaris exoculata*: an in-depth metagenomic investigation and discovery of *Zetaproteobacteria*. *Environ Microbiol* 2014; **16**: 2723–2738.

105. Ponnudurai R, Sayavedra L, Kleiner M, Heiden SE, Thürmer A, Felbeck H, et al. Genome sequence of the sulfur-oxidizing Bathymodiolus thermophilus gill endosymbiont. *Stand Genomic Sci* 2017; **12**: 50.

106. Ponnudurai R, Kleiner M, Sayavedra L, Petersen JM, Moche M, Otto A, et al. Metabolic and physiological interdependencies in the *Bathymodiolus azoricus* symbiosis. *ISME J* 2017; **11**: 463–477.

107. Fenchel T. Studies on the decomposition of organic detritus derived from the turtle grass *Thalassia testudinum*. *Limnol Oceanogr* 1970; **15**: 14–20.

108. Fenchel TM, Riedl RJ. The sulfide system: a new biotic community underneath the oxidized layer of marine sand bottoms. *Mar Biol* 1970; **7**: 255–268.

109. Reise K, Ax P. A meiofaunal 'thiobios' limited to the anaerobic sulfide system of marine sand does not exist. *Mar Biol* 1979; **54**: 225–237.

110. Dahl C, Friedrich C, Kletzin A. Sulfur Oxidation in Prokaryotes. *Encyclopedia of Life Sciences*. 2008. John Wiley & Sons, Ltd, Chichester, UK.

111. Weber PM, Moessel F, Paredes GF, Viehboeck T, Vischer NOE, Bulgheresi S. A bidimensional segregation mode maintains symbiont chromosome orientation toward its host. *Curr Biol* 2019; **29**: 3018-3028.e4.

112. Schwedt A, Kreutzmann AC, Polerecky L, Schulz-Vogt HN. Sulfur respiration in a marine chemolithoautotrophic *Beggiatoa* strain. *Front Microbiol* 2012; **2**: 276.

113. Nyström T, Neidhardt FC. Cloning, mapping and nucleotide sequencing of a gene encoding a universal stress protein in *Eschericha coli*. *Mol Microbiol* 1992; **6**: 3187–3198.

114. Aldsworth TG, Sharman RL, Dodd CER. Bacterial suicide through stress. *Cell Mol Life*

Sci . 1999. Springer. , **56**: 378–383

115. Nyström T. Not quite dead enough: on bacterial life, culturability, senescence, and death. *Arch Microbiol* . 2001. , **176**: 159–164

116. Nyström T. Translational fidelity, protein oxidation, and senescence: lessons from bacteria. *Ageing Res Rev* . 2002. Elsevier. , **1**: 693–703

117. Sat B, Reches M, Engelberg-Kulka H. The *Escherichia coli mazEF* suicide module mediates thymineless death. *J Bacteriol* 2003; **185**: 1803–1807.

118. Weber H, Engelmann S, Becher D, Hecker M. Oxidative stress triggers thiol oxidation in the glyceraldehyde-3- phosphate dehydrogenase of *Staphylococcus aureus*. *Mol Microbiol* 2004; **52**: 133–140.

119. Page R, Peti W. Toxin-antitoxin systems in bacterial growth arrest and persistence. *Nat Chem Biol* 2016; **12**: 208–214.

120. Hoor AT ten. Cell yield and bioenergetics of *Thiomicrospira denitrificans* compared with *Thiobacillus denitrificans*. *Antonie Van Leeuwenhoek* 1981; **47**: 231–243.

121. Sorokin DY, Tourova TP, Antipov AN, Muyzer G, Kuenen JG. Anaerobic growth of the haloalkaliphilic denitrifying sulfur-oxidizing bacterium *Thialkalivibrio thiocyanodenitrificans* sp. nov. with thiocyanate. *Microbiology* 2004; **150**: 2435–2442.

122. Nunoura T, Takaki Y, Kazama H, Kakuta J, Shimamura S, Makita H, et al. Physiological and genomic features of a novel sulfur-oxidizing gammaproteobacterium belonging to a previously uncultivated symbiotic lineage isolated from a hydrothermal vent. *PLoS One* 2014; **9**: e104959.

123. Justin P, Kelly DP. Growth kinetics of *Thiobacillus denitrificans* in anaerobic and aerobic chemostat culture. *J Gen Microbiol* 1978; **107**: 123–130.

124. Mitchell JH, Leonard JM, Delaney J, Girguis PR, Scott KM. Hydrogen does not appear to be a major electron donor for symbiosis with the deep-sea hydrothermal vent tubeworm Riftia pachyptila. *Appl Environ Microbiol* 2019; **86**: e01522-19.

125. Scott KM, Cavanaugh CM. CO2 uptake and fixation by endosymbiotic chemoautotrophs from the bivalve *Solemya velum*. *Appl Environ Microbiol* 2007; **73**:

1174–1179.

126. Woyke T, Teeling H, Ivanova NN, Huntemann M, Richter M, Gloeckner FO, et al. Symbiosis insights through metagenomic analysis of a microbial consortium. *Nature* 2006; **443**: 950–955.

127. Wood AP, Aurikko JP, Kelly DP. A challenge for 21st century molecular biology and biochemistry: what are the causes of obligate autotrophy and methanotrophy? *FEMS Microbiol Rev* 2004; **28**: 335–352.

128. Tal S, Okon Y. Production of the reserve material poly-β-hydroxybutyrate and its function in *Azospirillum brasilense* Cd. *Can J Microbiol* 1985; **31**: 608–613.

129. Natarajan K, Kishore L, Babu CR. Characteristics of NaCl stress associated proteins of *Rhizobium* under varying cultural conditions. *J Basic Microbiol* 1995; **35**: 413–420.

130. Steinbüchel A, Füchtenbusch B. Bacterial and other biological systems for polyester production. *Trends Biotechnol* 1998; **16**: 419–427.

131. Kadouri D, Burdman S, Jurkevitch E, Okon Y. Identification and isolation of genes involved in poly(beta-hydroxybutyrate) biosynthesis in *Azospirillum brasilense* and characterization of a *phbC* mutant. *Appl Environ Microbiol* 2002; **68**: 2943–2949.

132. Ayub ND, Pettinari MJ, Ruiz JA, López NI. A polyhydroxybutyrate-producing *Pseudomonas* sp. isolated from antarctic environments with high stress resistance. *Curr Microbiol* 2004; **49**: 170–174.

133. Kadouri D, Jurkevitch E, Okon Y, Castro-Sowinski S. Ecological and agricultural significance of bacterial polyhydroxyalkanoates. *Crit Rev Microbiol* 2005; **31**: 55–67.

134. Obruca S, Sedlacek P, Krzyzanek V, Mravec F, Hrubanova K, Samek O, et al. Accumulation of poly(3-hydroxybutyrate) helps bacterial cells to survive freezing. *PLoS One* 2016; **11**: e0157778.

135. Obruca S, Sedlacek P, Mravec F, Krzyzanek V, Nebesarova J, Samek O, et al. The presence of PHB granules in cytoplasm protects non-halophilic bacterial cells against the harmful impact of hypertonic environments. *N Biotechnol* 2017; **39**: 68–80.

136. Slaninova E, Sedlacek P, Mravec F, Mullerova L, Samek O, Koller M, et al. Light

scattering on PHA granules protects bacterial cells against the harmful effects of UV radiation. *Appl Microbiol Biotechnol* 2018; **102**: 1923–1931.

137. Kim JK, Won YJ, Nikoh N, Nakayama H, Han SH, Kikuchi Y, et al. Polyester synthesis genes associated with stress resistance are involved in an insect-bacterium symbiosis. *Proc Natl Acad Sci U S A* 2013; **110**: E2381–E2389.

138. Hamad MA, Austin CR, Stewart AL, Higgins M, Vázquez-Torres A, Voskuil MI. Adaptation and antibiotic tolerance of anaerobic *Burkholderia pseudomallei*. *Antimicrob Agents Chemother* 2011; **55**: 3313–3323.

139. Claessen D, Errington J. Cell wall deficiency as a coping strategy for stress. *Trends Microbiol* 2019; **27**: 1025–1033.

140. Antia NJ, Harrison PJ, Oliveira L. The role of dissolved organic nitrogen in phytoplankton nutrition, cell biology and ecology. *Phycologia* 1991; **30**: 1–89.

141. Walsh P, Wang Y, Campbell C, Boeck DG, Wood C. Patterns of nitrogenous waste excretion and gill urea transporter mRNA expression in several species of marine fish. *Mar Biol* 2001; **139**: 839–844.

142. Beckers G, Bendt AK, Krämer R, Burkovski A. Molecular identification of the urea uptake system and transcriptional analysis of urea transporter- and urease-encoding genes in Corynebacterium glutamicum. *J Bacteriol* 2004; **186**: 7645–7652.

143. Ashoori M, Saedisomeolia A. Riboflavin (vitamin B2) and oxidative stress: a review. *Br J Nutr* 2014; **111**: 1985–1991.

144. Gould RL, Pazdro R. Impact of supplementary amino acids, micronutrients, and overall diet on glutathione homeostasis. *Nutrients* 2019; **11**: 1056.

145. Carmel-Harel O, Storz G. Roles of the glutathione- and thioredoxin-dependent reduction systems in the *Escherichia coli* and *Saccharomyces cerevisiae* responses to oxidative stress. *Annu Rev Microbiol* 2000; **54**: 439–461.

146. Williams CH. Mechanism and structure of thioredoxin reductase from Escherichia coli. *FASEB J* 1995; **9**: 1267–1276.

147. Vanoni MA, Curti B. Glutamate synthase: a complex iron-sulfur flavoprotein. *Cell Mol*

Life Sci 1999; **55**: 617–638.

148. Liang J, Han Q, Tan Y, Ding H, Li J. Current advances on structure-function relationships of pyridoxal 5′-phosphate-dependent enzymes. *Front Mol Biosci* 2019; **6**: 4.

149. Banerjee R, Ragsdale SW. The many faces of vitamin B12: catalysis by cobalamin-dependent enzymes. *Annu Rev Biochem* 2003; **72**: 209–247.

150. Fontecave M, Atta M, Mulliez E. S-adenosylmethionine: nothing goes to waste. *Trends Biochem Sci* 2004; **29**: 243–249.

151. Caro AA, Cederbaum AI. Antioxidant properties of S-adenosyl-l-methionine in Fe2+-initiated oxidations. *Free Radic Biol Med* 2004; **36**: 1303–1316.

152. Imhoff JF. Diversity of Anaerobic Anoxygenic Phototrophic Purple Bacteria. *Modern Topics in the Phototrophic Prokaryotes*. 2017. Springer International Publishing, Cham, pp 47–85.

1214 **Figure legends**

1215

1216 **Figure 1. Median gene expression levels of selected *Ca.* T. oneisti metabolic**
1217 **processes under anoxic, sulfidic (AS) versus oxic (O) conditions.** All genes involved in
1218 a particular process were manually collected and median expression levels (log_2TPMs,
1219 transcripts per kilobase million) per condition and process after 24 h of incubation are shown
1220 (horizontal bold lines). Importantly, metabolic processes include both differentially and
1221 constitutively expressed genes, and the total number of genes considered are indicated at
1222 the bottom of each process. For the specific assignment of genes see Data S1. Note that for
1223 the processes designated as 'Amino acids', 'Storage' and 'Vitamins & cofactors' only the
1224 expression of the biosynthesis genes was considered. Boxes indicate interquartile ranges
1225 (25%-75%), whiskers refer to the minimum and maximum expression values, respectively.
1226 The individual processes are ordered according to the difference in median expression
1227 between AS and O conditions, i.e. denitrification (far left) had the largest difference in
1228 median expression between the two conditions, with higher median expression in the AS
1229 condition, whereas urea utilization (far right) had the largest difference in median expression,
1230 with higher median expression in the O condition. Metabolic processes were considered
1231 highly expressed when their median expression level was above 5.2 log_2TPM (dashed grey
1232 line), which represents the median expression of all expressed protein-coding genes (n = 4
1233 591) under both conditions. CBB cycle: Calvin-Benson-Bassham cycle.

1234

1235 **Figure 2. Oxidation of stored sulfur is coupled to denitrification but decoupled from**
1236 **CO_2 fixation under anoxic conditions.** (A) Heatmap visualizing differentially expressed
1237 genes (2-fold change, FDR ≤ 0.05) involved in sulfur oxidation, denitrification and CO_2
1238 fixation via the Calvin-Benson-Bassham cycle between the anoxic, sulfidic (AS) and oxic (O)
1239 conditions after 24 h of incubation. Expression levels are visualized by displaying mean-
1240 centered log_2TPMs (transcripts per kilobase million). Upregulation is indicated in red,
1241 downregulation in blue. Genes are ordered by function in the respective metabolic pathways.

1242 S: sulfur, FCC: flavocytochrome c, Dsr: dissimilatory sulfite reductase, APS: adenylylsulfate,
1243 Qmo: quinone-interacting membrane-bound oxidoreductase, Hdr: heterodisulfide reductase,
1244 Nap: periplasmic nitrate reductase, Nir: cd_1 nitrite reductase, qNor: quinol-dependent nitric
1245 oxide reductase, Nos: nitrous oxide reductase, Siroheme synt.: siroheme biosynthesis
1246 (heme d precursor), RuBisCo su.: ribulose-1,5-bisphosphate carboxylase/oxygenase small
1247 subunit, PPi-PFK: PPi-dependent phosphofructokinase, Ru5P epi.: ribulose-5-phosphate 3-
1248 epimerase. (B) Relative elemental sulfur (S^0) content in ectosymbionts as determined by
1249 Raman microspectroscopy after 24 h incubations under anoxic, sulfidic (AS; red dots),
1250 anoxic without added sulfide (A, black dots) or oxic (O) conditions (O; dark blue: hypoxic,
1251 light blue: oxygen-saturated). Each dot refers to the value obtained from measuring an
1252 individual ectosymbiont cell; 50 cells were measured per condition. Horizontal lines display
1253 medians, boxes show the interquartile ranges (25-75%), whiskers indicate minimum and
1254 maximum values and different lower-case letters indicate significant differences among
1255 conditions ($p < 0.05$, Wilcoxon rank sum test). (C) Relative ^{13}C isotope content of symbiotic
1256 *L. oneistus* as determined by EA-IRMS after 24 h incubations with ^{13}C-labeled bicarbonate.
1257 Dots refer to the values determined in individual measurements (comprising 50 worms per
1258 measurement, for further details see Table S2). Horizontal lines indicate means, error bars
1259 correspond to standard deviations. The categories ^{12}C-live and ^{13}C-dead refer to the natural
1260 isotope abundance control and the dead control, respectively. Colors were assigned to the
1261 distinct incubations as shown in panel (B). Different lower-case letters indicate significant
1262 differences among conditions (one-way ANOVA, Tukey's post-hoc test, $p < 0.05$).
1263

1264 **Figure 3. Nitrogen fixation and urea utilization genes are upregulated under oxic**
1265 **conditions.** The heatmap only shows genes that were differentially expressed (2-fold
1266 change, FDR ≤ 0.05) between anoxic, sulfidic (AS) and oxic (O) conditions after 24 h of
1267 incubation. Expression levels are displayed as mean-centered log_2TPMs (transcripts per
1268 kilobase million). Upregulation is indicated in red, downregulation in blue. Genes are ordered

1269 by function in the respective metabolic pathway. Cofactor synt.: cofactor biosynthesis,
1270 Urease acc. proteins: urease accessory proteins.
1271
1272 **Figure 4. Expression of genes involved in various stress responses and vitamin**
1273 **biosynthesis is upregulated in under oxic conditions and coincides with fewer**
1274 **dividing symbiont cells.** (A) Heatmaps showing stress-related genes and genes involved
1275 in biosynthesis of vitamins and cofactors, as determined on the transcript level. Expression
1276 levels are visualized by displaying mean-centered $\log_2$TPMs (transcripts per kilobase
1277 million). Upregulation is indicated in red, and downregulation in blue. Genes are ordered by
1278 function in the respective metabolic pathways. Heavy metal rest.: heavy metal resistance.
1279 (B) Bars show the mean percentage of dividing *Ca.* T. oneisti cells upon 24 h incubations
1280 under anoxic, sulfidic (AS) or oxic conditions (O). The latter condition includes both, cells
1281 incubated under hypoxic and oxygen-saturated conditions. A total of 658, 1 009, and 1 923
1282 cells were counted for the AS, hypoxic and oxygen-saturated condition, respectively. Error
1283 bars indicate 95% confidence intervals (Fisher's exact test).
1284
1285 **Figure 5. Schematic representation of *Ca.* T. oneisti's suggested metabolism in deep**
1286 **anoxic and superficial sand.** Note that the illustrated processes likely occur under both
1287 anoxic, sulfidic (AS) and oxic (O) conditions, but the model highlights those proposed to be
1288 dominant in one condition over the other. Our study suggests that in anoxic, sulfidic
1289 sediment zones (left) the ectosymbiont performs enhanced anaerobic sulfur oxidation
1290 coupled to nitrate reduction to nitrogen gas (dentrification). Other electron acceptors (such
1291 as DMSO) are also being reduced. The storage compound PHA serves as a carbon source
1292 (in addition to CO_2) and as an additional electron donor. Host-derived phospholipids (P-
1293 lipids) may be incorporated into the ectosymbiont's membrane to increase permeability. In
1294 superficial, oxygenated zones (right), oxygen triggers a global stress response that not only
1295 consumes energy and dampens proliferation, but also requires vitamin biosynthesis which
1296 might increase the demand for nitrogen. Small organic carbon compounds (C_{org}), putatively

1297 excreted by the host, contribute to energy generation (and carbon) via aerobic respiration.
1298 Together with autotrophic CO_2 fixation, C_{org} increases carbon availability thereby allowing for
1299 PHA biosynthesis. Heme and other essential nutrients may be directly or indirectly
1300 transferred to the host.

Figure 1

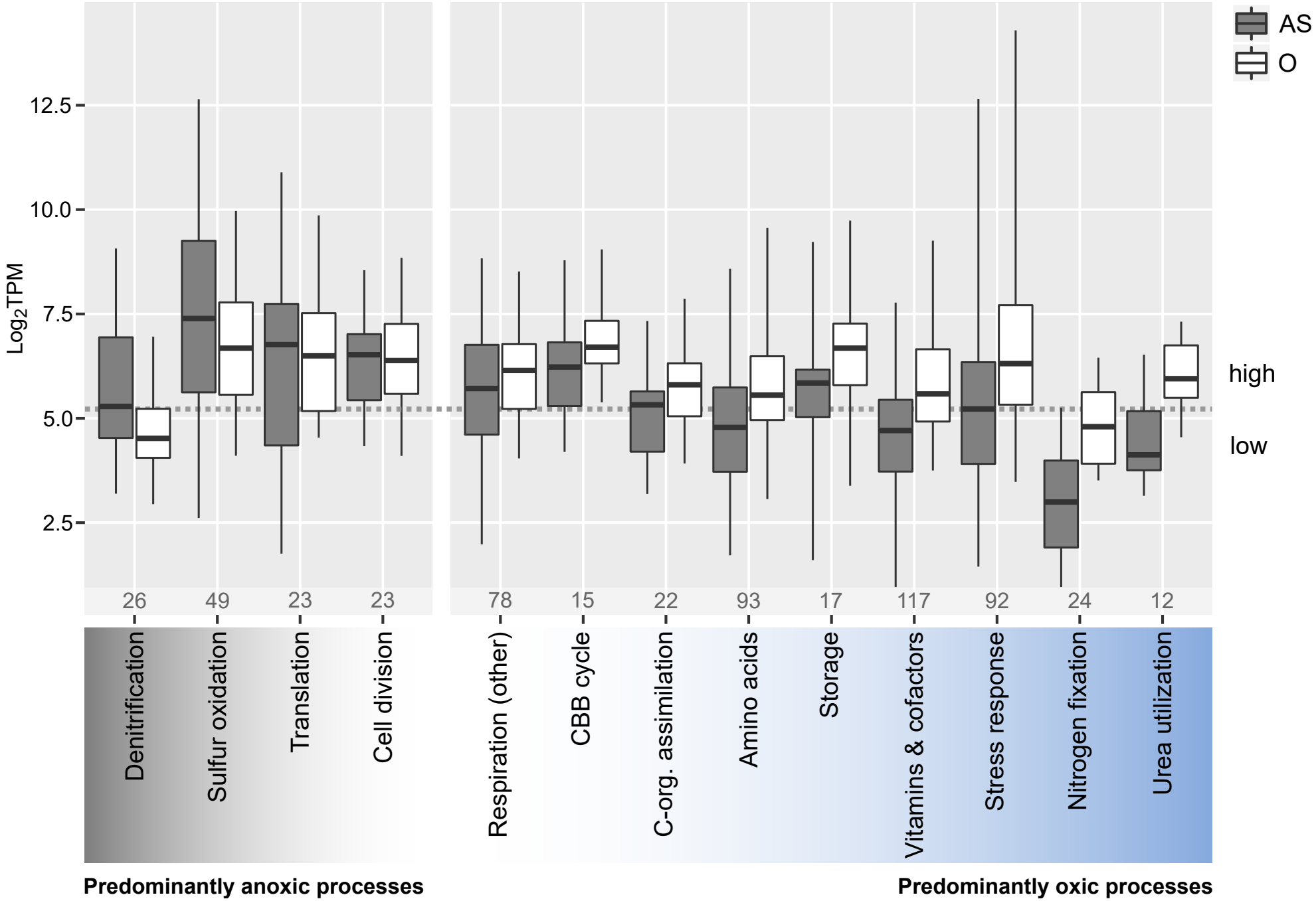
AS
O
12.5
10.0
7.5
5.0
2.5
Log2TPM
high
low
26
49
23
23
78
15
22
93
17
117
92
24
12
Denitrification
Sulfur oxidation
Translation
Cell division
Respiration (other)
CBB cycle
C-org. assimilation
Amino acids
Storage
Vitamins & cofactors
Stress response
Nitrogen fixation
Urea utilization
Predominantly anoxic processes
Predominantly oxic processes

Figure 2

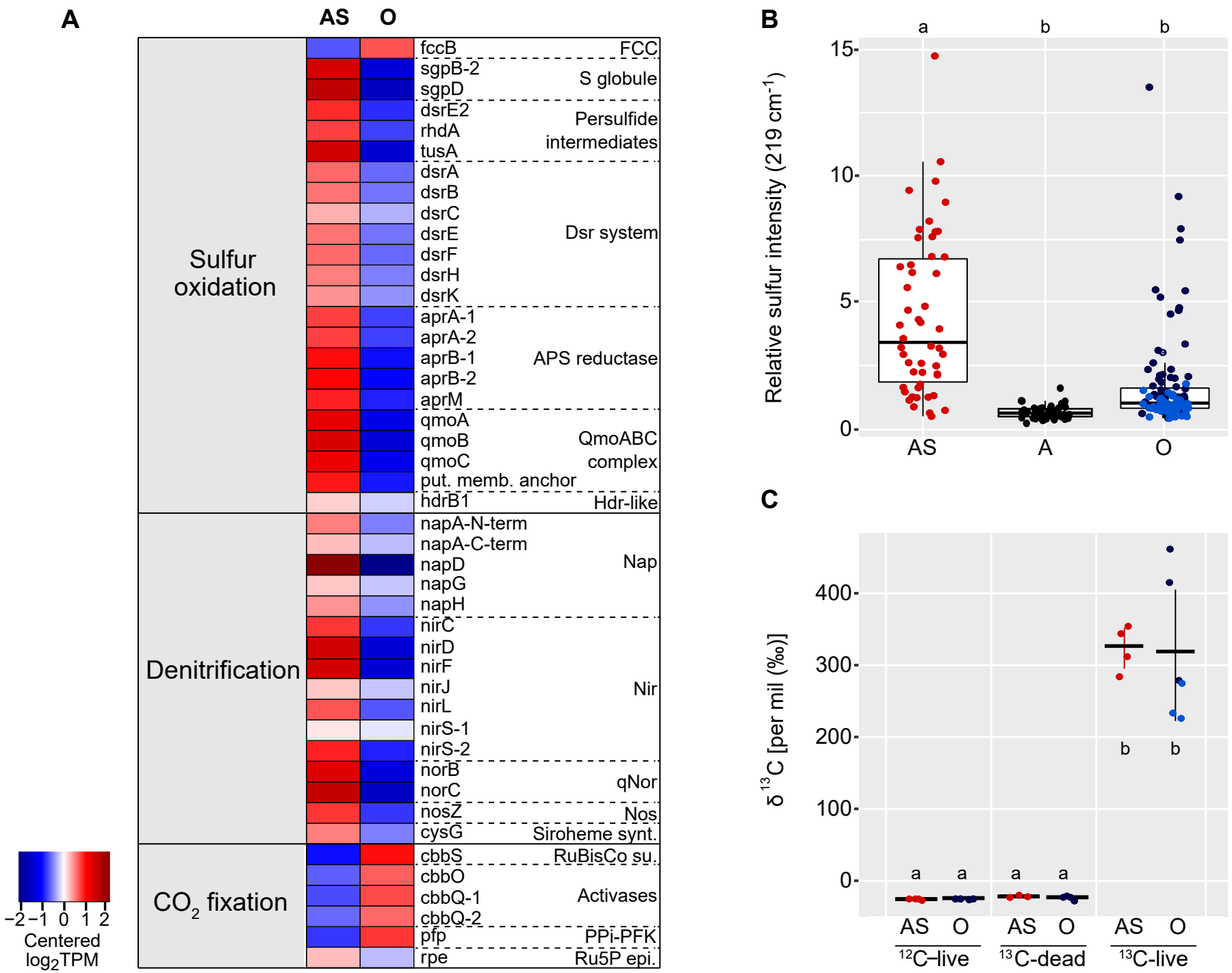
A
AS
O
Sulfur oxidation
Denitrification
CO2 fixation
fccB
FCC
sgpB-2
sgpD
S globule
dsrE2
rhdA
tusA
Persulfide intermediates
dsrA
dsrB
dsrC
dsrE
dsrF
dsrH
dsrK
Dsr system
aprA-1
aprA-2
aprB-1
aprB-2
aprM
APS reductase
qmoA
qmoB
qmoC
put. memb. anchor
QmoABC complex
hdrB1
Hdr-like
napA-N-term
napA-C-term
napD
napG
napH
Nap
nirC
nirD
nirF
nirJ
nirL
nirS-1
nirS-2
Nir
norB
norC
qNor
nosZ
Nos
cysG
Siroheme synt.
cbbS
RuBisCo su.
cbbO
cbbQ-1
cbbQ-2
Activases
pfp
PPi-PFK
rpe
Ru5P epi.
−2 −1 0 1 2
Centered log2TPM
B
Relative sulfur intensity (219 cm-1)
a
b
b
AS
A
O
C
δ13C [per mil (‰)]
a
a
a
a
b
b
AS
O
AS
O
AS
O
12C–live
13C-dead
13C-live

Figure 3

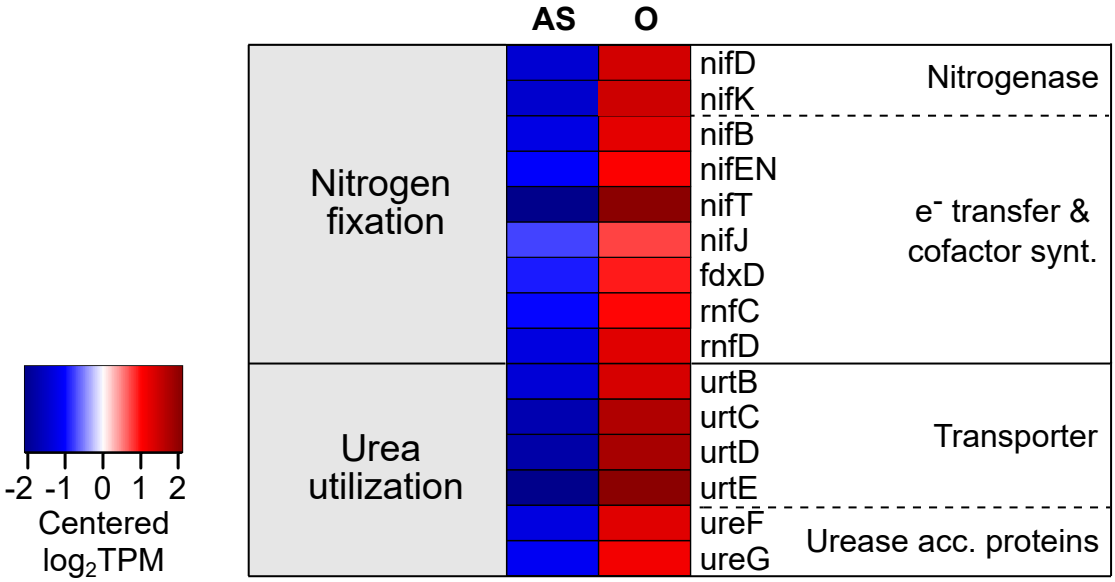
AS
O
Nitrogen fixation
Urea utilization
nifD
nifK
nifB
nifEN
nifT
nifJ
fdxD
rnfC
rnfD
urtB
urtC
urtD
urtE
ureF
ureG
Nitrogenase
e⁻ transfer & cofactor synt.
Transporter
Urease acc. proteins
-2 -1 0 1 2
Centered log2TPM

Figure 4

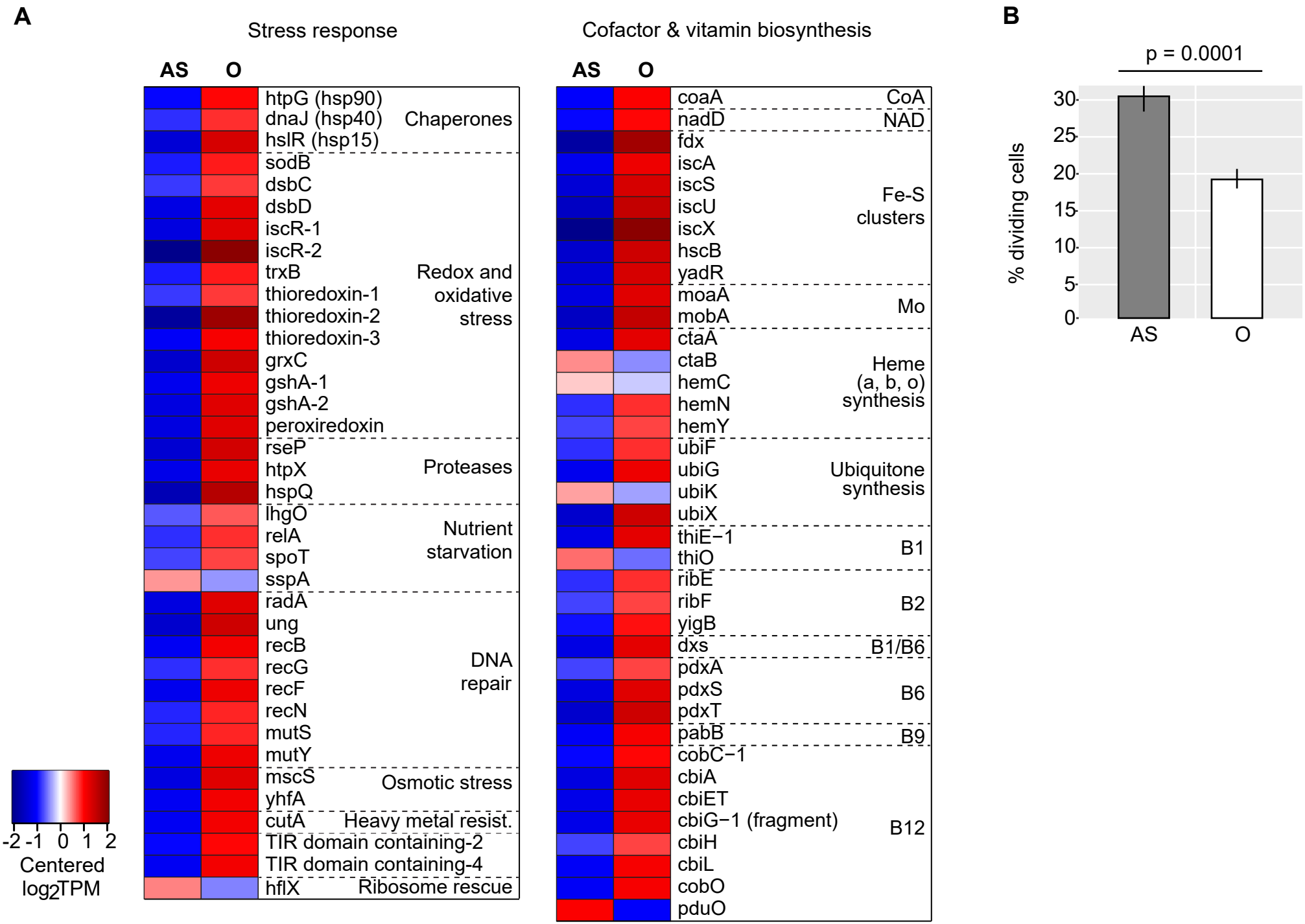
A
Stress response
AS
O
htpG (hsp90)
dnaJ (hsp40)
hslR (hsp15)
Chaperones
sodB
dsbC
dsbD
iscR-1
iscR-2
trxB
thioredoxin-1
thioredoxin-2
thioredoxin-3
grxC
gshA-1
gshA-2
peroxiredoxin
Redox and oxidative stress
rseP
htpX
hspQ
Proteases
lhgO
relA
spoT
sspA
Nutrient starvation
radA
ung
recB
recG
recF
recN
mutS
mutY
DNA repair
mscS
yhfA
Osmotic stress
cutA
Heavy metal resist.
TIR domain containing-2
TIR domain containing-4
hflX
Ribosome rescue
-2 -1 0 1 2
Centered log2TPM
Cofactor & vitamin biosynthesis
AS
O
coaA
CoA
nadD
NAD
fdx
iscA
iscS
iscU
iscX
hscB
yadR
Fe-S clusters
moaA
mobA
Mo
ctaA
ctaB
hemC
hemN
hemY
Heme (a, b, o) synthesis
ubiF
ubiG
ubiK
ubiX
Ubiquitone synthesis
thiE−1
thiO
B1
ribE
ribF
yigB
B2
dxs
B1/B6
pdxA
pdxS
pdxT
B6
pabB
B9
cobC−1
cbiA
cbiET
cbiG−1 (fragment)
cbiH
cbiL
cobO
pduO
B12
B
p = 0.0001
% dividing cells
30
25
20
15
10
5
0
AS
O

Figure 5

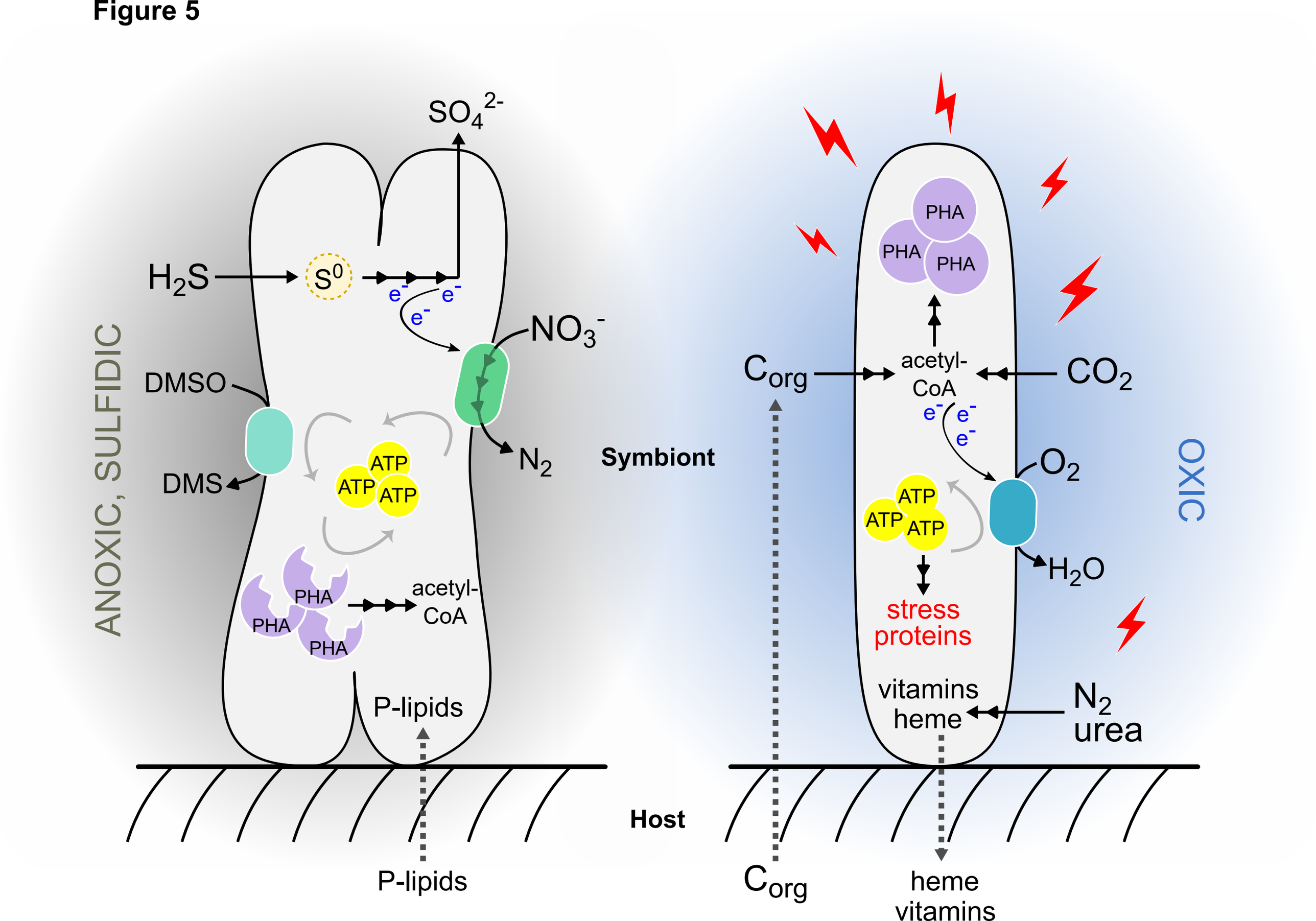
ANOXIC, SULFIDIC
OXIC
Symbiont
Host
SO_4^{2-}
H_2S
S^0
e^-
NO_3^-
DMSO
DMS
N_2
ATP
PHA
acetyl-CoA
P-lipids
C_{org}
CO_2
O_2
H_2O
stress proteins
vitamins
heme
N_2
urea
heme
vitamins